Structural Setting of the 2008 Mw 7.9 Wenchuan, China, Earthquake

Judith Hubbard, John H. Shaw, Yann Klinger

Bulletin of the Seismological Society of America, Vol. 100, No. 5B, pp. 2713–2735, November 2010, doi: 10.1785/0120090341

Structural Setting of the 2008 M_w 7.9 Wenchuan, China, Earthquake

by Judith Hubbard, John H. Shaw, and Yann Klinger

Abstract The 2008 M_w 7.9 Wenchuan earthquake ruptured an imbricate thrust system in the Longmen Shan range, which forms the eastern boundary of the Tibetan Plateau. We use seismic reflection data and surface geology to construct geologic cross sections and a three-dimensional (3D) fault model in the range front. The rupture was complex, with slip on both the steeply dipping Beichuan fault and the more shallowly dipping Pengguan fault, which appear to merge at depth. In contrast, only the Beichuan fault ruptured in the north, with the transition near a lateral fault offset. Thus, the earthquake involved multiple thrust splays and breached a significant segment boundary. To investigate the tectonic setting of the earthquake, we extend our previous measurements of crustal shortening (Hubbard and Shaw, 2009) into the interior of the range and show that shortening correlates with topography. This suggests that upper-crustal shortening can produce the high topography of the Longmen Shan without calling on other uplift mechanisms. Based on this understanding, we model the thrust belt as a critical taper wedge, to assess what rock and fault strengths are required to explain the topographic slopes within the range front and basin. The low taper within the basin is consistent with a weak detachment ($\delta_f \approx 0.1$), while a slightly stronger ($\delta_f \approx 0.3$–0.4) detachment is necessary to explain the higher taper of the range front. This difference may relate to the localization of the detachment within a Triassic evaporite sequence within the basin, while the faults beneath the range front are rooted in Precambrian metasedimentary or igneous rocks. Critical taper theory implies that shortening in the range front where the 2008 Wenchuan earthquake occurred is many times greater than in the basin, consistent with our shortening measurements. We examine the implications of these findings for seismic hazard assessment in the region and in other active mountain belts around the world.

Introduction

The 2008 M_w 7.9 Wenchuan earthquake occurred in the Sichuan Province of central China, along the Longmen Shan mountain belt, which defines the eastern margin of the Tibetan Plateau (Fig. 1). Seismological data indicate that the rupture initiated in the southern Longmen Shan and propagated unilaterally toward the northeast for ~250 km, with equivalent magnitudes of thrust and dextral motion (Lin *et al.*, 2009; Xu *et al.*, 2009). The earthquake caused more than 80,000 fatalities, left more than 1.5 million people homeless, and produced enormous economic losses (Stone, 2008). The rupture occurred in a region with no prior historic earthquakes of comparable size and in a region with only modest amounts of horizontal shortening measured by geodesy (Chen *et al.*, 2000; Shen *et al.*, 2005).

The Wenchuan earthquake had several important characteristics that provide insights into the nature of large earthquakes in mountain belts and the tectonic processes that have developed the Longmen Shan. First, the earthquake occurred in a fold belt that many considered to be largely inactive, with lower-crustal inflation invoked to explain the topography in the absence of significant active crustal shortening. Second, the earthquake had a very complex source geometry, rupturing not one, but two northwest-dipping faults that form part of an imbricate stack, and extending laterally across a major segment boundary (Figs. 1, 2). Finally, the earthquake occurred deep in the interior of the mountain belt, 200 km northwest of the toe of the fold-and-thrust belt in the Sichuan basin, and thus has been termed out-of-sequence (e.g., Liu-Zeng *et al.*, 2009). These attributes clearly had major impacts on the level of damage generated by the earthquake. The rupture of multiple faults and the earthquake's ability to breach a major lateral, geometric segment boundary enabled it to be very large, thereby increasing the magnitude and duration of hazardous ground shaking. In addition, the fact that the earthquake did not involve the frontal faults in the fold-and-thrust belt likely spared the largest population centers, such as the city of Chengdu, from major damage, but had severe consequences for the towns in the mountainous region where the earthquake occurred.

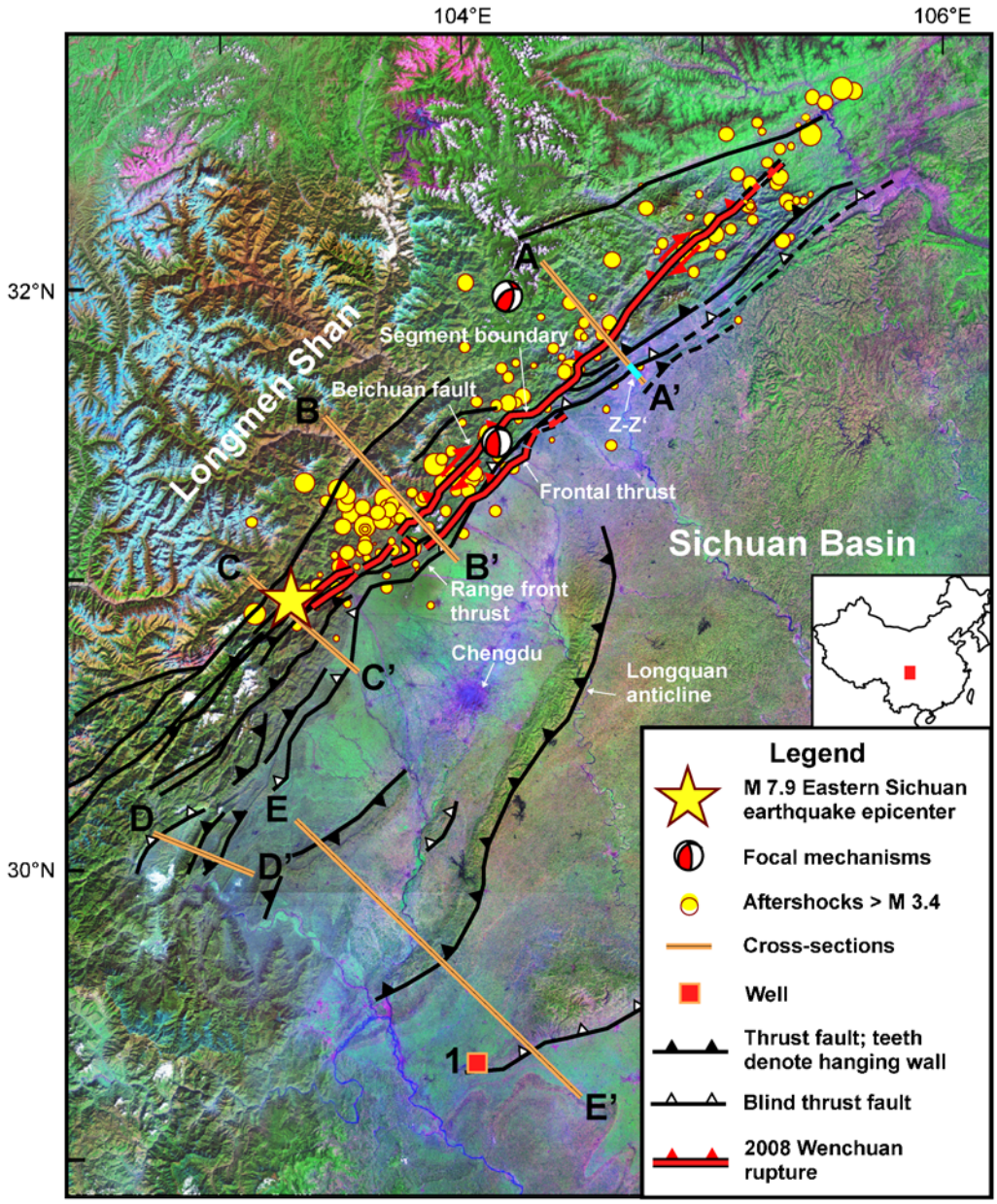

Figure 1. Landsat image of the Longmen Shan and western Sichuan basin, showing the epicenter and focal mechanisms of the 2008 Wenchuan earthquake, aftershocks, and major faults. Cross sections A-A' through E-E' are geological interpretations based on seismic reflection profiles and surface geological data. Cross section Z-Z' is shown in Figure 10. Emergent and blind thrusts are distinguished, as are the Beichuan fault and the portion of the frontal fault system that ruptured in the 2008 Wenchuan earthquake. Well 1 is shown in Figure 16. Focal mechanisms were obtained from the U.S. Geological Survey (northern focal mechanism) and the Global Centroid Moment Tensor Project (southern) (see the Data and Resources section). (Figure after Hubbard and Shaw, 2009.) The color version of this figure is available only in the electronic edition.

In this paper, we define the structural setting of the Wenchuan earthquake and use these insights to examine the nature of deformation in the Longmen Shan and the Sichuan basin. First, we develop a comprehensive, three-dimensional (3D) model of the structures in the Longmen Shan, including the faults that ruptured in the Wenchuan earthquake. We examine the changes in the geometry of the rupture and associated faults along strike, and explore the geometric and kinematic interactions of the various fault splays that comprised the earthquake rupture. The Wenchuan earthquake demonstrates the ability of thrust fault earthquakes to involve multiple thrust splays and rupture across significant lateral segment boundaries, which has implications for earthquake hazards in this region and in other mountain belts around the world.

We then examine the shortening recorded on faults in the upper crust extending through the Sichuan basin and into the Longmen Shan. These shortening patterns are compared with

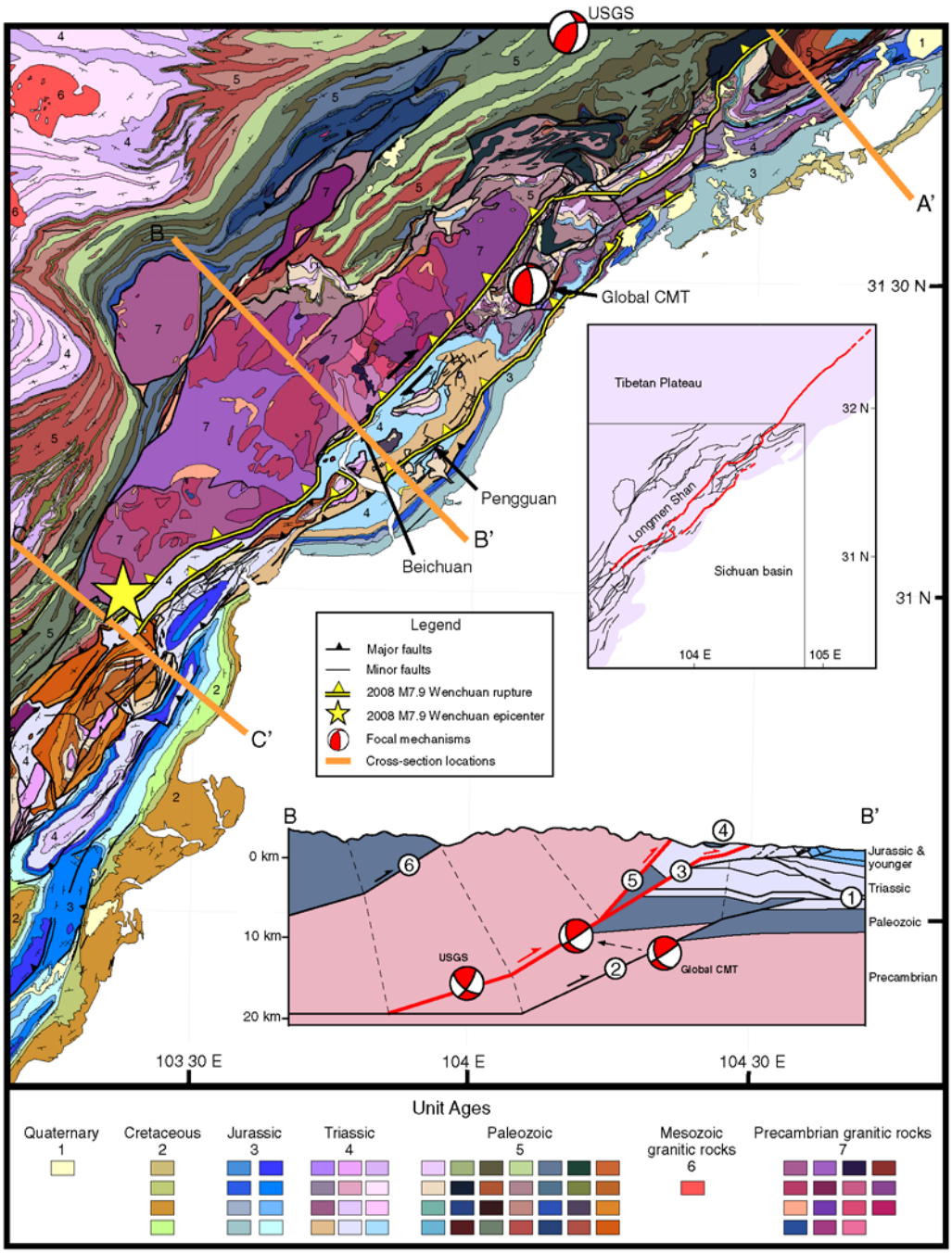

Figure 2. Geological map of the Longmen Shan, with inset showing the location of the map relative to the complete surface rupture. The epicenter, focal mechanisms (obtained from the U.S. Geological Survey and the Global Centroid Moment Tensor Project; see Data and Resources section), and surface rupture are distinguished. Cross section shows geological interpretation of line B-B', with lower-hemisphere projections of the focal mechanisms viewed along strike; shades in the cross section are a simplified representation of those on the geological map. The original Global CMT location appears to be inconsistent with mapped faults; a dashed arrow points to a more reasonable location on the cross section. The six main structures of the range are numbered: (1) upper detachment system, (2) Range Front thrust, (3) frontal fault system, (4) frontal klippen, (5) Beichuan fault, and (6) Wenchuan fault. For descriptions see the text. The "Unit Ages" legend gives the rough ages of the rocks shown in the map; numbers 1–7 on the map represent rough age classifications. The inset show major faults and surface rupture. The color version of this figure is available only in the electronic edition.

topography to assess if crustal shortening or lower-crustal inflation is responsible for the topography of the mountain belt. This analysis extends our previously published results (Hubbard and Shaw, 2009), and employs a large dataset of industry seismic reflection data (Fig. 3), combined with geologic maps and surface rupture data (Fig. 2), to develop balanced cross sections. We then show that the fold-and-thrust belt can be modeled as a critical taper wedge using reasonable

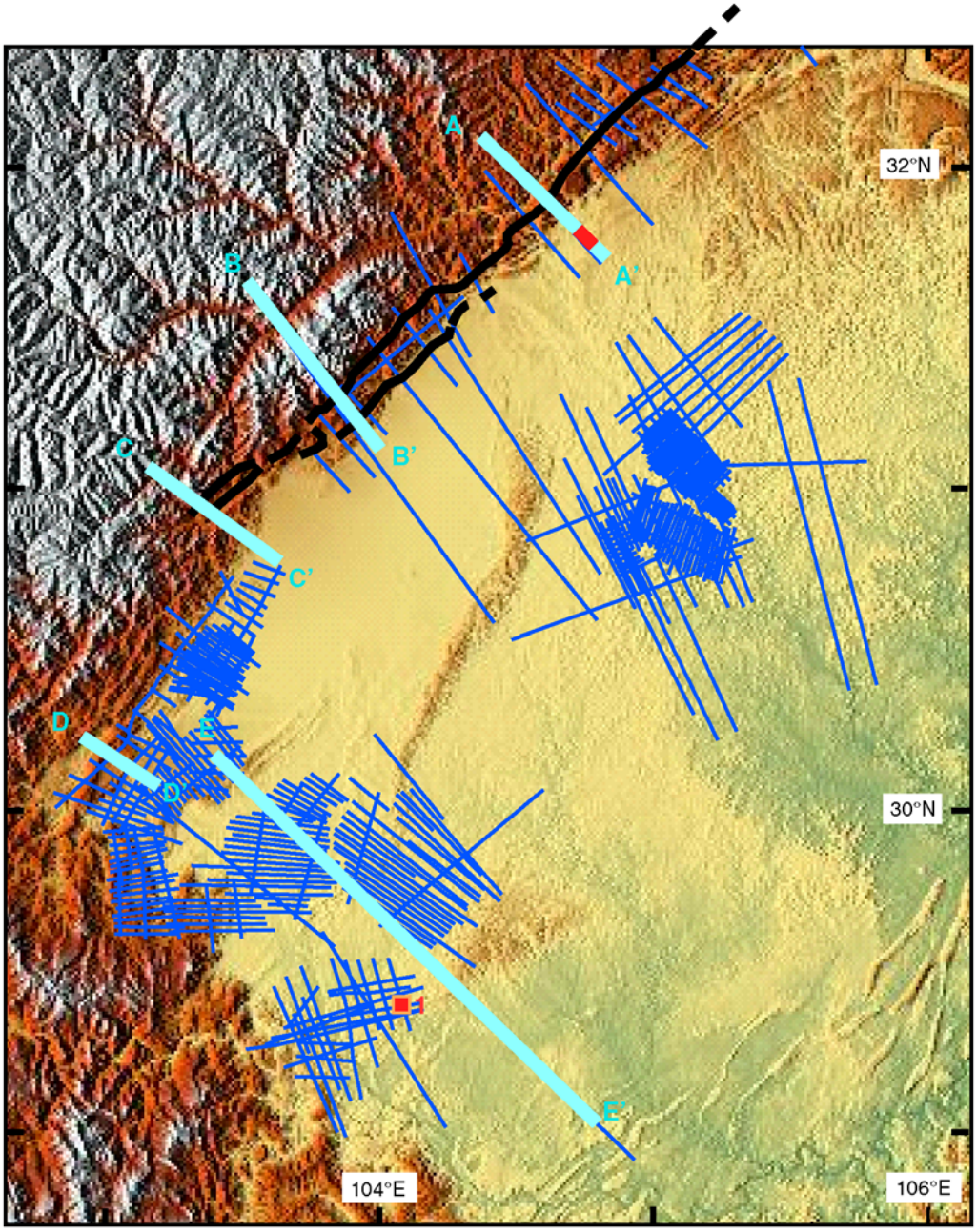

Figure 3. Topographic map of the Longmen Shan and western Sichuan basin. Thin dark lines show the locations of available seismic reflection profiles used to produce our geological cross sections; thick light lines show the locations of interpreted cross sections. Cross section Z-Z' (Figs. 1, 10) is distinguished over cross section A-A'. Square indicates location of Well 1 (Fig. 16). Thick black line shows the 2008 Wenchuan surface rupture from Xu *et al.* (2009). The color version of this figure is available only in the electronic edition.

values of crustal and basal detachment strength. The fold belt exhibits two distinct tapers, one in the range front and a second in the basin, which likely reflect differences in basal detachment strengths. Finally, we explore the implications of these findings for regional earthquake hazards.

Character of the Wenchuan Rupture

Prior to the Wenchuan earthquake, interpretations of satellite imagery suggested active thrusting and strike slip on faults in the Longmen Shan (Tapponnier and Molnar, 1977), and geomorphic observations of offset terraces identified slip (dominantly dextral) on the Pengguan fault within the last 1000 yr, and of offset terraces and other landforms on the Beichuan fault within the last 12–13 ka (Densmore *et al.*, 2007). However, very low seismicity along the range front suggested that the faults in the range were relatively inactive, although several large historical earthquakes ($>M7$) ruptured the Min Jiang and Huya faults to the north of the Longmen Shan (Chen *et al.*, 1994).

The M_w 7.9 Wenchuan earthquake demonstrated that the faults in the range front are both currently active and capable of generating large earthquakes. The rupture initiated at about 16 km depth, propagating unilaterally upward and to the northeast. Seismic source inversions show that the rupture can be divided into two subevents. The first subevent occurred near Yingxiu and exhibited oblique, right-lateral thrust slip, while the second occurred to the northeast near Beichuan and was dominated by right-lateral slip (e.g., Ji and Hayes, 2008; Sladen, 2008; Shen *et al.*, 2009). Field investigations show that the Wenchuan earthquake ruptured both the Beichuan and Pengguan faults along the central segment of the Longmen Shan thrust belt (Liu-Zeng *et al.*, 2009; Xu *et al.*, 2009). The Beichuan and Pengguan faults have similar north-northeasterly strikes and dip to the northwest; they represent two faults within an imbricate stack that comprise the structure of the range front (Fig. 2) (Hubbard and Shaw, 2009). The Beichuan fault dips steeply (>60°) to the northwest at the surface and is interpreted to sole to a basal detachment below the rupture surface (Fig. 2). Based on the results reported in Liu-Zeng *et al.* (2009) and Xu *et al.* (2009), the average vertical offset along the Beichuan rupture zone is 2–4 m, with one anomalous scarp ~10 m high, and local maxima of 5–6 m; the maximum right-lateral offset is 4.4–6.8 m. The Pengguan fault trace is located about 12 km east of the southern part of the Beichuan fault rupture (Fig. 2). The Pengguan fault dips moderately (≈30°) to the west, with the surface rupture dominated by thrust offsets with only minor right-lateral slip (<1 m). The maximum vertical offset across the coseismic scarp is 2.9–3.7 m, and the vertical offset decreases gradually to the northeast (Liu-Zeng *et al.*, 2009; Xu *et al.*, 2009). These observations confirm that the Wenchuan earthquake involved coseismic ruptures on multiple faults that represent part of an imbricate thrust stack, implying that the source geometry was complicated. The Beichuan fault, which lies in the hinterland and is thus the more steeply dipping member of the faults that ruptured, accommodated a significant component of strike slip. In contrast, the Pengguan fault, which lies to the foreland and dips more gently, accommodated nearly pure dip slip.

To further explore the nature of the earthquake source geometry, we developed a series of geologic cross sections and a comprehensive 3D representation of the fault systems in the Longmen Shan range front and the western Sichuan basin, including the faults that ruptured in the Wenchuan earthquake. We integrated geologic maps, detailed maps of surface ruptures, including surficial estimates of fault dips, and measurements of uplift and lateral displacements from Xu *et al.* (2009), earthquake hypocenters and focal mechanisms relocated using double-difference methods (Pei *et al.*, 2008), an extensive grid of seismic reflection profiles acquired by the petroleum industry (Figs. 3, 4, 5, 6), and logs

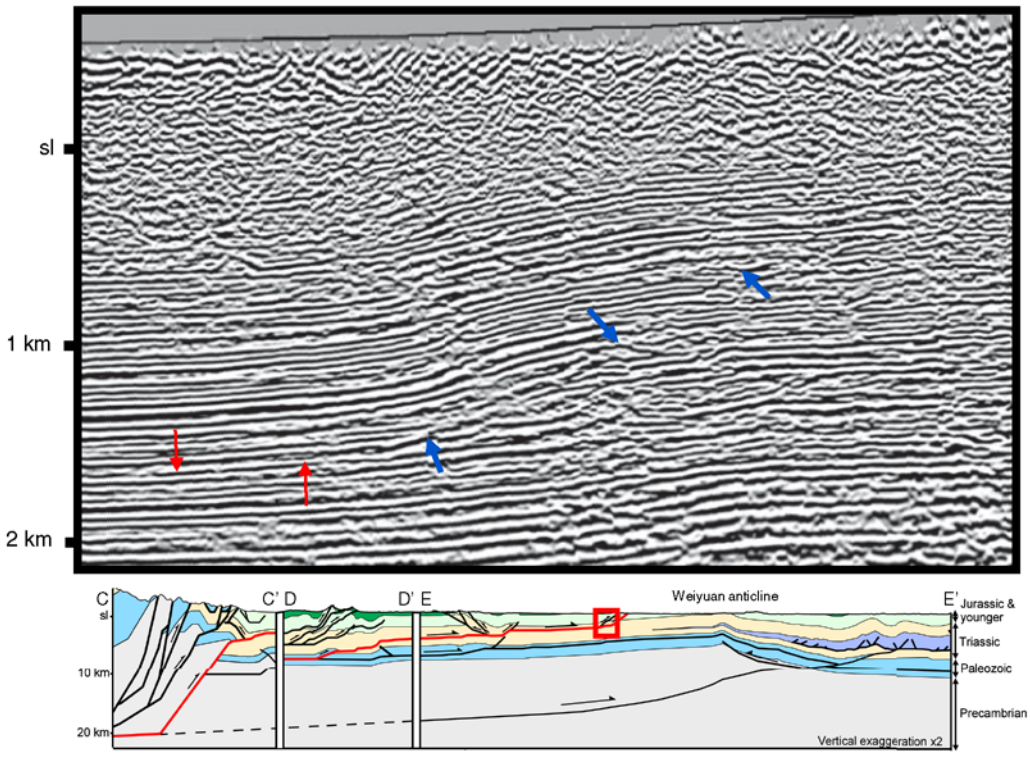

Figure 4. Sample seismic reflection profile crossing the Longquan anticline. Thick arrows point to the location of the thrust fault; thin arrows pick out the detachment. Lower cross section is a composite of cross sections C-C', D-D', and E-E'; box shows the location of the seismic profile and interpretation. Depth conversion was performed using a 2D velocity model derived from stacking velocities. Note that the seismic data is 1:1, while the cross section is vertically exaggerated (x2). The color version of this figure is available only in the electronic edition.

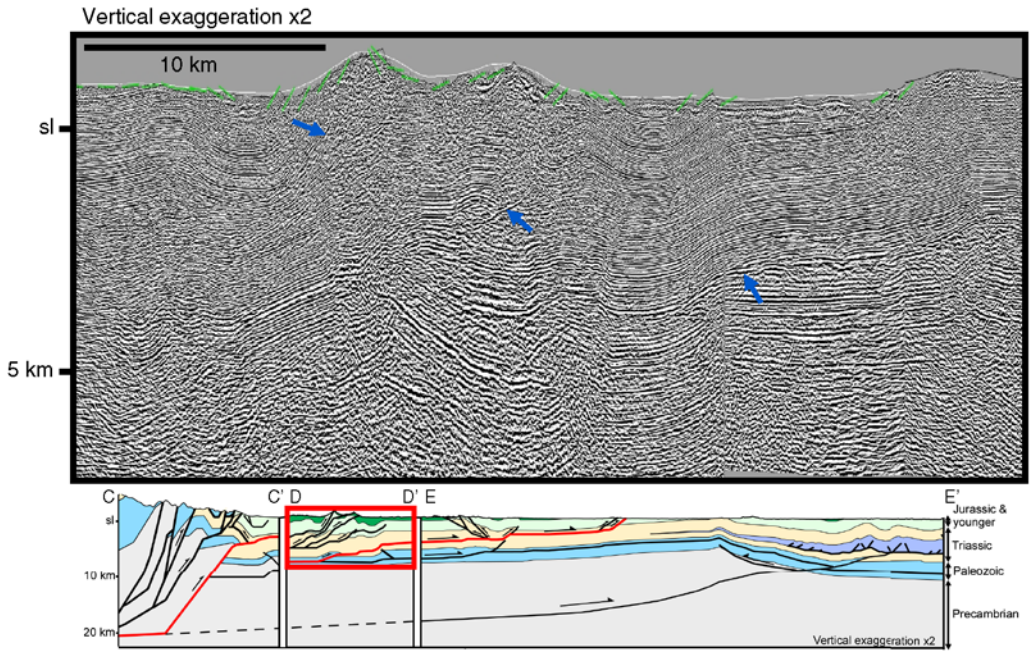

Figure 5. Sample seismic reflection profile crossing the foothills region of the Longmen Shan (cross section D-D'). Arrows point to faults visible in the seismic reflection profile. Lower cross section is a composite of cross sections C-C', D-D', and E-E'; box shows the location of the seismic profile and interpretation. Depth conversion was performed using a 2-D velocity model derived from stacking velocities. Note that both the seismic data and the cross section are vertically exaggerated (x2). The color version of this figure is available only in the electronic edition.

from petroleum wells that define stratigraphic tops and seismic velocities.

The geologic section shown in Figure 2 defines the six main fault systems that have accommodated deformation in the Longmen Shan: (1) the detachment system that underlies the Sichuan basin at a few km depth and rises to the surface on thrust faults within the basin (Fig. 4); (2) the Range Front thrust, a blind fault that connects the detachment system in the Sichuan basin with a much deeper detachment under the Longmen Shan (Fig. 6); (3) the frontal thrusts, including the Pengguan and Hanwang faults, which crop out at the range front; (4) the frontal klippen, which extend along strike southeast of the Beichuan fault and bring Paleozoic rocks above Triassic; (5) the Beichuan fault, which is the main fault that ruptured in the Wenchuan earthquake; and (6) the Wenchuan fault, a steeply dipping fault that lies northwest of the Beichuan fault. The faults and basal detachment in the Sichuan basin are directly imaged by high-quality seismic reflection data. The basin detachment dips slightly to the west toward the range front and lies at depths ranging from about 3 to 4 km. As this detachment approaches the range front, seismic reflection data show that it displaces a Mesozoic and Paleozoic section in its hanging wall above Mesozoic strata in its footwall. The hanging wall strata are folded into a broad anticline that has direct surface expression (Fig. 7). The stratigraphic juxtaposition and hanging-wall fold geometry imply that the detachment steps down to the west, forming a thrust ramp that we term the Range Front thrust. We interpret the dip of this thrust ramp (33°) using fault-bend folding theory (Suppe, 1983) based on the observed hanging-wall cutoff angle (β-35°), the fold shape (axial angle γ-75°), and the dip of the fault above the bend (4°). The maximum depth of the Range Front thrust is not directly constrained. The mapped traces and surface dips of the Pengguan (≈30°NW) and Beichuan (> 60°NW) faults imply that the two structures intersect one another at a depth well above the mainshock hypocenter. Moreover, the location of the hypocenter and the dip of its preferred nodal plane (35° from the Global CMT catalog) suggest that the Beichuan fault shallows its dip with depth. This fault geometry is consistent with the presence of a major synclinorium that lies to the northwest of the Beichuan and Wenchuan faults (Figs. 2, 7). Based on fault-related folding theories (Suppe, 1983; Shaw *et al.*, 2005), we suggest that a shallowing of the dip of the Beichuan thrust to a detachment between ~16–20 km is consistent with the earthquake data, the surface fault constraints, and the location and geometry of the synclinorium. While other solutions for the fault geometry at depth are likely permissible, we suggest that this interpretation is compatible with tomographic observations of a low-velocity zone at depths of 16–26 km beneath the range (Huang *et al.*, 2009), as well as the fact that very few earthquakes have occurred beneath those depths (Li *et al.*, 2010).

To represent the geometries of these fault systems in three dimensions, we georeferenced and integrated these geological and geophysical data and interpretations into GOCAD (Mallet, 1992), a 3D geologic CAD tool that is suitable for modeling fault geometries and other types of

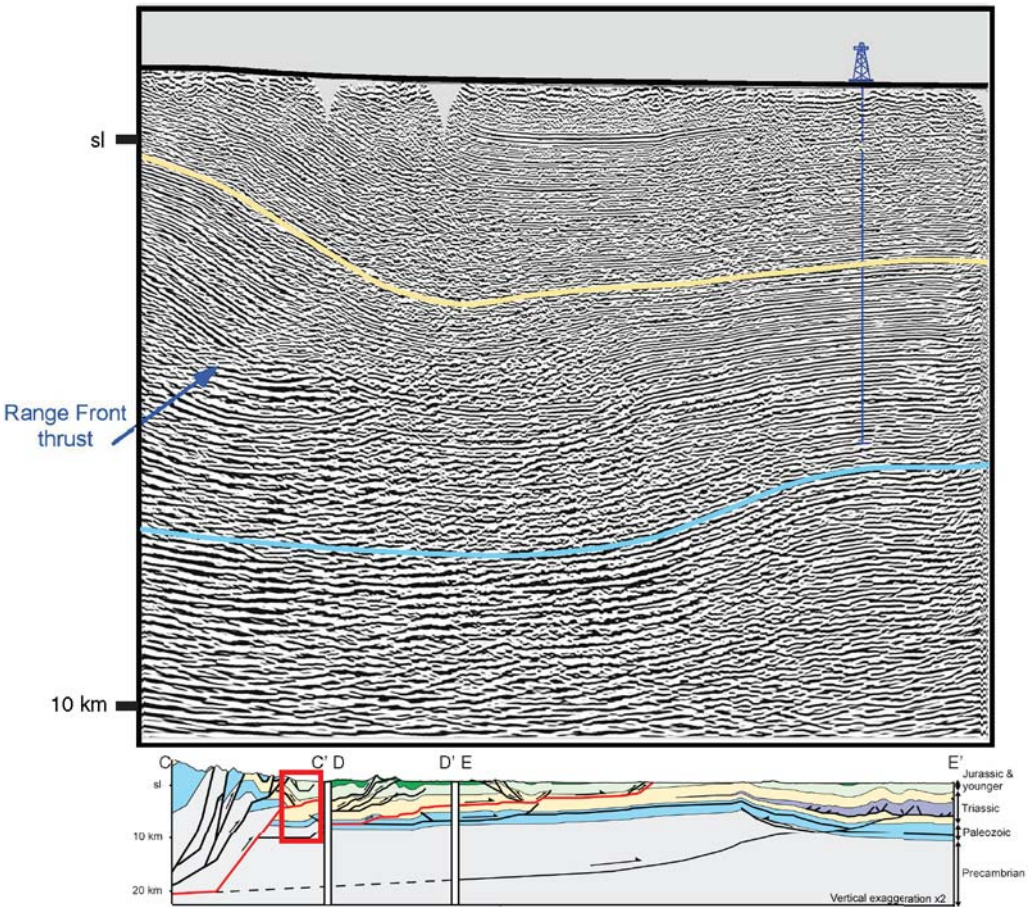

Figure 6. Sample seismic reflection profile showing the upper part of the blind Range Front thrust. Upper horizon shows the top of the Triassic; lower shows the top of the Paleozoic. Dipping units (e.g., Top Triassic) above the flat detachment constrain the dip of the Range Front thrust following our understanding of kinematic fault-bend folding (Suppe, 1983; Shaw *et al.*, 2005). Lower cross section is a composite of cross sections C-C', D-D', and E-E'; box shows the location of the seismic profile and interpretation. Note that the seismic data is 1:1, while the cross section is vertically exaggerated (x2). The color version of this figure is available only in the electronic edition.

structural analysis. We used these data to build triangulated surface representations to define the complex fault shapes within the Longmen Shan following the approach of Plesch *et al.* (2007). Our model includes all of the major fault systems described in the cross sections, with the exception of the frontal klippen, as these are clearly inactive. Figure 8b shows an image of our model in perspective view, with the faults that ruptured in the Wenchuan earthquake. This figure emphasizes the changes of the geometry of the fault system along strike, with two faults rupturing in the southern section and only one in the north. The 3D geometries of the faults are also shown as contour maps (Fig. 9).

These 3D fault geometries and surface rupture patterns indicate that some degree of slip partitioning occurred during the Wenchuan earthquake. The earthquake ruptured both the steeply dipping (~40–60°) Beichuan fault and the more shallowly dipping (~30°) Pengguan fault. Field measurements indicate that the Pengguan fault was almost complete dip slip, while the Beichuan fault accommodated only slightly more dip slip than strike slip. Slip partitioning is a process by which oblique motions are accommodated in the near surface, with lateral displacements occurring on steeply dipping strike-slip faults and dip slip occurring on more shallowly dipping faults (e.g., Gaudemer *et al.*, 1995; Bowman *et al.*, 2003). In the case of the Wenchuan earthquake, the slip partitioning was not perfect: while the shallowly dipping Pengguan fault did rupture with dip slip, the steeply dipping Beichuan fault is not vertical and accommodated mixed strike-slip and dip-slip motion. Nevertheless, the lateral component of slip was accommodated on the more steeply dipping of the two faults. Our analysis suggests that the Beichuan fault acquired its steep dip by a process of imbrication, based on the observation that strata in its footwall are folded by underlying thrust faults. Moreover, our 3D analysis suggests that the Beichuan and Pengguan faults merge at depth and, therefore, that the deepest levels of faulting, below the fault branching point, likely accommodate oblique slip. We note that the difference in slip partitioning between the southern and northern rupture zones is also consistent with finite fault models (e.g., Ji and Hayes, 2008; Sladen, 2008), which

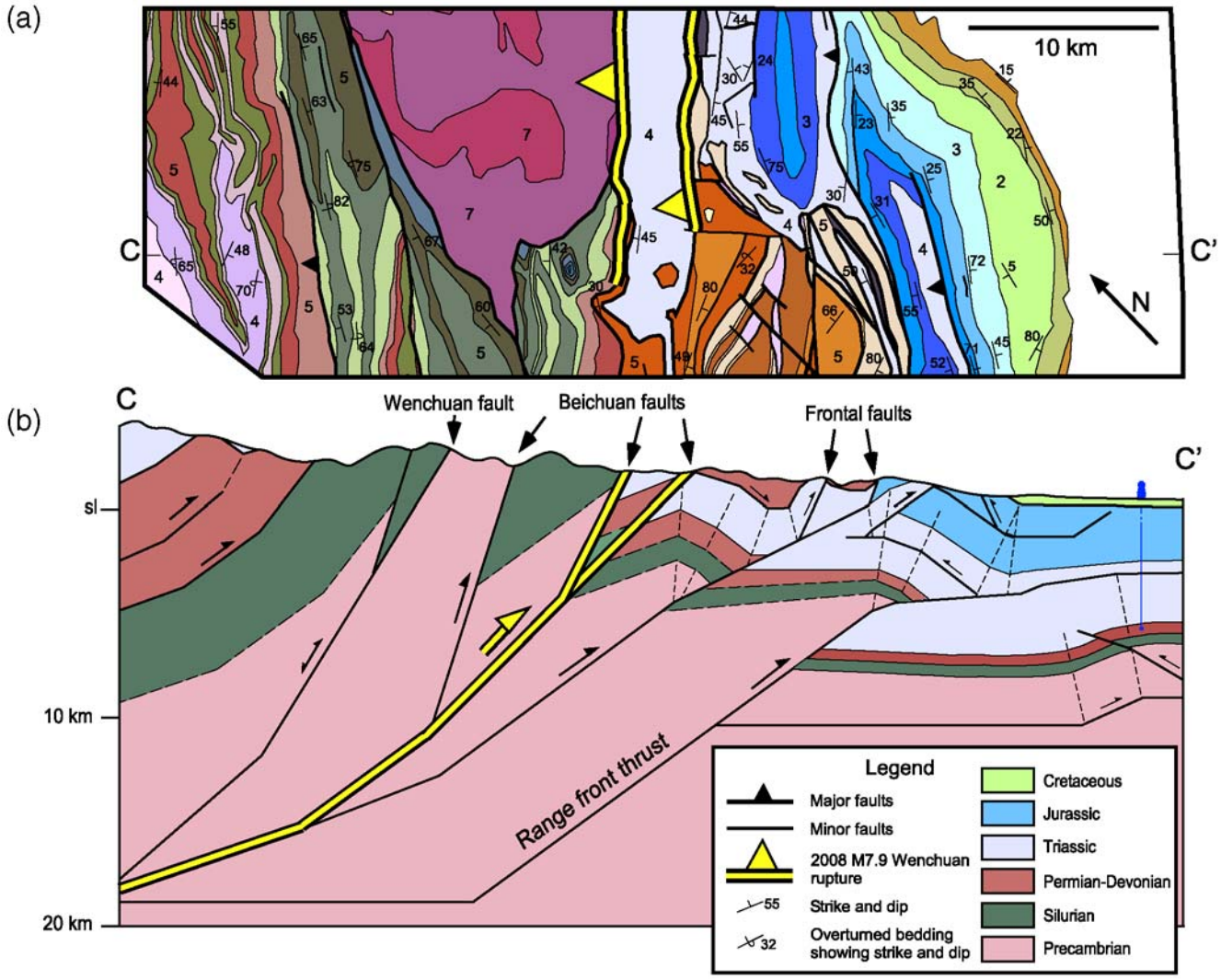

Figure 7. (a) Strip of geological map showing the surface data used to constrain cross section C-C' (see Fig. 2 for full map). (b) Cross section C-C', shaded to roughly correspond to the map. Note that the right side of the cross section is further constrained by the seismic data shown in Figure 5. The shades and numbers in the strip map are the same as in Figure 2. The Beichuan fault splits into several splays in this location, of which two ruptured. The color version of this figure is available only in the electronic edition.

shows that the southern zone exhibited oblique, right-lateral thrust slip producing slip partitioning along two faults, while the northern zone was dominated by right-lateral slip, with rupture along a single, steeply dipping fault. This behavior was also documented in the M_w 8–8.3 1927 Gulang earthquake, China (Gaudemer *et al.*, 1995), the M_w 7.6 1932 Changma earthquake, China (Peltzer *et al.*, 1998; Meyer *et al.*, 1998), the M_w 8.3 1957 Gobi–Altai earthquake, Mongolia (Baljinnyam *et al.*, 1993; Ritz *et al.*, 2003), and the M_w 7.8 2001 Kokoxili earthquake, China (King *et al.*, 2005). Nevertheless, such slip-partitioning events appear to be rare.

The Wenchuan earthquake rupture also exhibits significant changes in fault geometry along strike. The northern and southern parts of the Beichuan rupture are separated by an ~9–10 km wide right-stepping lateral offset previously mapped by Tapponnier and Molnar (1977); rupture between these segments highlighted a roughly east–west-trending tear fault (Fig. 1) (Xu *et al.*, 2009). The obliquity of the rupture suggests that the slip on this fault should have been largely dextral. Fault segmentation of this sort has been mapped in previous events (e.g., Spotila and Sieh, 1995; Haeussler *et al.*, 2004; Klinger *et al.*, 2006; Klinger, 2010). Wesnousky (2006) observed that the maximum dimension of fault steps across which strike-slip earthquakes rupture is about 4 km; this limit was upheld by Elliott *et al.* (2009). Zhang *et al.* (1999) examined normal faulting earthquakes in the Basin and Range Province and observed no events rupturing across discontinuities greater than 5 km (1915 Pleasant Valley). Wesnousky (2008) found that dip-slip events have ruptured through steps of 5–7 km, greater than for strike-slip earthquakes. The step in the Wenchuan earthquake is larger than all of these limits, however, implying that there may be important differences between the Wenchuan rupture and the more traditional strike-slip and dip-slip events used in

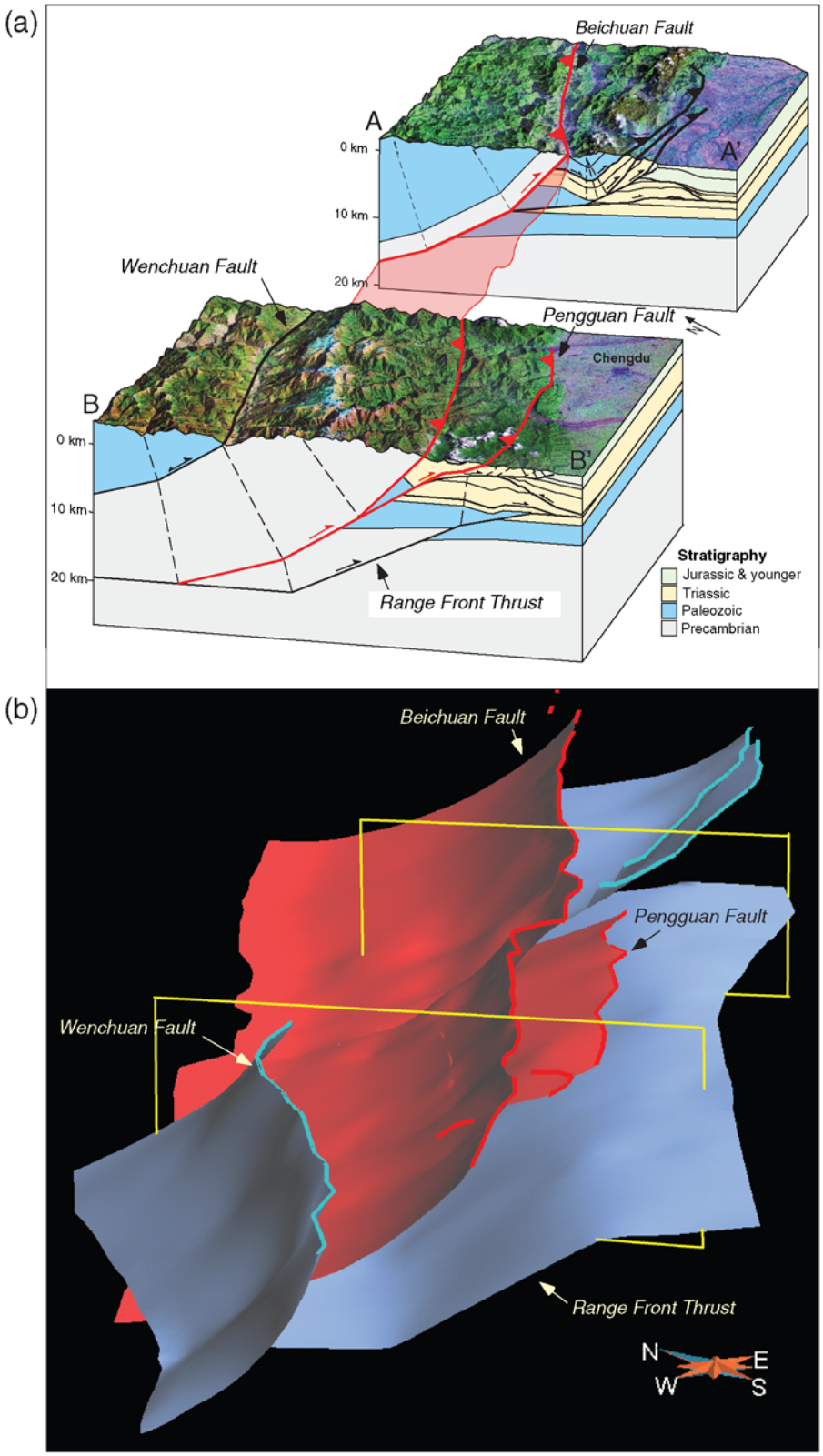

Figure 8. (a) Perspective view of the eastern Longmen Shan looking to the northeast, showing cross sections A-A' and B-B' of Figure 1. Major faults are shown. The surface shows a Landsat image draped on a DEM. (Figure after Xu *et al.*, 2009.) (b) View of the 3D model produced in GOCAD from the same perspective. Wenchuan rupture is composed of Beichuan and Pengguan faults; the upper detachment, Range Front thrust, lower detachment, northern frontal faults, and Wenchuan fault are also shown. Boxes indicate the locations of cross sections A-A' and B-B', which were used to construct the model. The color version of this figure is available only in the electronic edition.

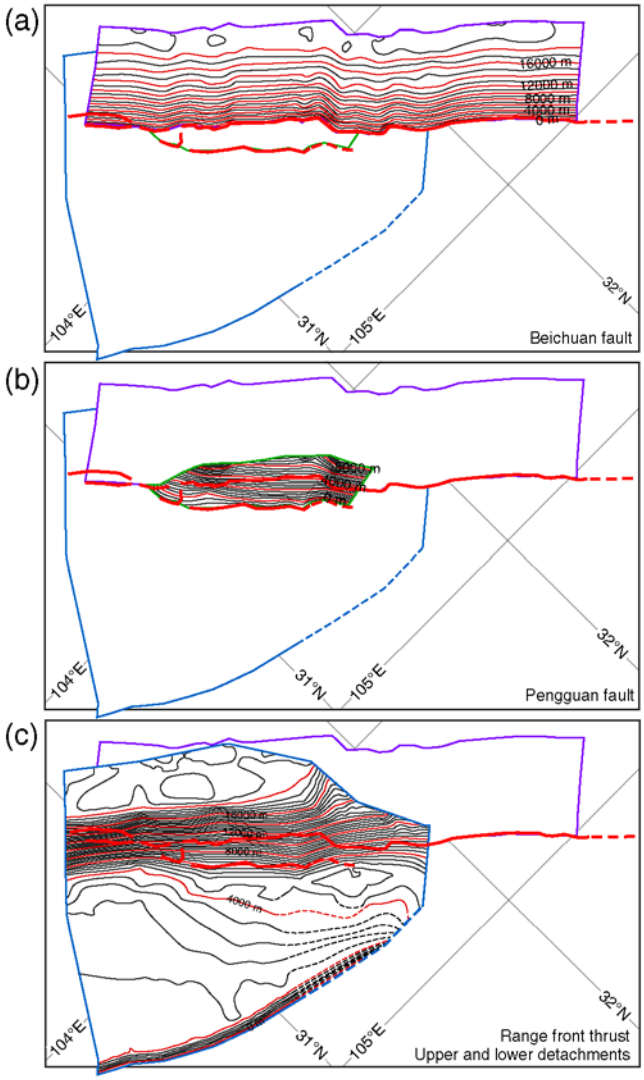

Figure 9. Contour maps taken from the 3D model, showing (a) the Beichuan fault, (b) the southern frontal fault, and (c) the upper detachment/Range Front thrust/lower detachment surface. The color version of this figure is available only in the electronic edition.

the Zhang *et al.* (1999),Wesnousky (2006), and Wesnousky (2008) analyses. This suggests that complex oblique-slip earthquakes, such as the Wenchuan event, may have higher limits to breaching segment boundaries than previously recognized. Possible explanations for this distinct behavior include the concept that long-lived or mature faults such as the Beichuan structure may have a greater ability to breach lateral segment boundaries than do less mature faults (Duan and Oglesby, 2006). Alternatively, our analysis suggests that these two segments of the Beichuan fault are linked in the subsurface (Figs. 8, 9), despite the change in elevation across this fault step and the disappearance of the Pengguan rupture (Xu *et al.*, 2009). While other interpretations may be viable, our results indicate that the surface offset between the two features may be a surficial feature and would presumably have little influence on the rupture path. This possibility emphasizes the importance of 3D fault models for understanding earthquake hazard, because geometric boundaries that appear to define fault segments at the surface may not pose boundaries to ruptures at depth.

Tectonic Setting of the Wenchuan Earthquake in the Longmen Shan

The Longmen Shan mountain range is at the center of a controversial debate about the rheology of the lower crust and the processes by which mountain belts grow. The Longmen Shan extends for more than 350 km along strike across central China and separates the Tibetan Plateau from the Sichuan basin. The mountain peaks rise 5500 m above the basin over a horizontal distance of about 70 km, exhibiting one of the highest reliefs of the Plateau margin. Many structures in the Longmen Shan show evidence of polyphase deformation, with both Mesozoic (largely Triassic) and Cenozoic age structures observed in outcrop and in the subsurface (Fig. 10). In many cases, such as in the Zhongba thrust sheet, Cenozoic structures have clearly reactivated older Mesozoic fault systems (Burchfiel *et al.*, 1995; Jia *et al.*, 2006; Li *et al.*, 2010). Exhumation rates imply that the present relief of the mountain belt has largely formed since the Miocene (Kirby *et al.*, 2002). However, geodetic studies (Chen *et al.*, 2000; Shen *et al.*, 2005; Meade, 2007), as well as geologic and geomorphic observations (Densmore *et al.*, 2007), generally agreed prior to the Wenchuan earthquake that east–west shortening across the range and within the basin was very limited (<3 mm/yr). These studies also indicate an important component of strike-slip deformation, at least since 10–15 ka. Moreover, the Longmen Shan lacks a typical foreland basin, a depression caused by plate loading that typically occurs in front of fold-and-thrust belts (Burchfiel *et al.*, 1995; Burchfiel *et al.*, 2008). As a result, basic and controversial questions persist about how this relief was created and is sustained, fueling debate about how the broader Tibetan Plateau formed.

Several authors have interpreted that the Longmen Shan formed by crustal faulting and shortening (e.g., Meyer *et al.*, 1998; Tapponnier *et al.*, 2001). However, to explain the apparent lack of geodetically observed shortening, others have proposed that they are maintained by dynamic pressure from lower-crustal flow (Bird, 1991; Royden *et al.*, 1997; Burchfiel, 2004). This hypothesis argues that lower-crustal material flowing outward from the center of the plateau is buttressed by the old, strong lithosphere that underlies the Sichuan basin, pushing up the crust above and maintaining steep topography through dynamic pressure. This model does not require substantial horizontal shortening at the surface, because the upper crust is largely uplifted, but not laterally displaced, by the lower-crustal motion (Royden *et al.*, 1997; Clark and Royden, 2000; Clark *et al.*, 2005; Cook and Royden, 2008).

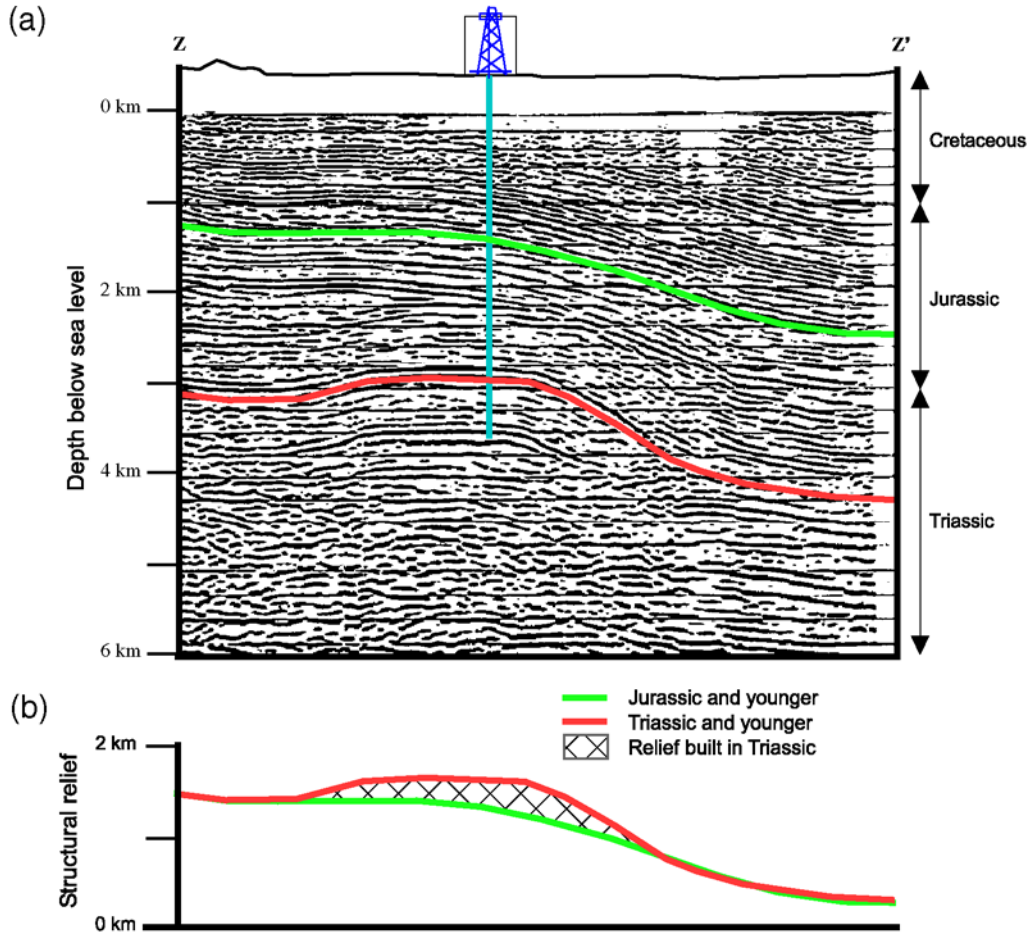

Figure 10. (a) Seismic reflection profile Z-Z' showing the Zhongba anticline. Lower horizon shows deformation of the Triassic units; upper horizon shows deformation of the Jurassic units. (b) Structural relief of the Triassic and Jurassic. Note that the Triassic has slightly more structural relief than the Jurassic. This indicates that there have been at least two phases of deformation (one in the Triassic, one Cenozoic) along this cross section. Location of profile is shown in Figure 1. The color version of this figure is available only in the electronic edition.

Crustal Shortening and Topography of the Longmen Shan

In a recent study by our group, we established that topography, crustal shortening, and structural relief are strongly correlated in the Longmen Shan foothills, and that the magnitudes of shortening and uplift are more than adequate to generate the topography (Fig. 11) (Hubbard and Shaw, 2009). In this paper, we extend our measurements of upper-crustal shortening further into the Longmen Shan range front based on our new cross sections and 3D fault model to improve our understanding of how the mountain belt developed.

We measure the percent of shortening recorded in the upper crust along two cross sections (D-D' and E-E') extending from the southern Sichuan basin into the foothills of the Longmen Shan. Shortening is estimated in each area of the section by restoring hanging-wall and footwall fault cutoffs and palinspastically restoring strata within folds (after Dahlstrom, 1969). We note very low shortening values of 1.6–2.7% within the basin, increasing toward the range front to a maximum of 37% in the foothills. This correlates with the increase in topography from the Sichuan basin into the foothills. Extending these measurements farther to the west into the high topography of the Longmen Shan, however, poses a specific challenge because we cannot measure the precise amount of shortening that produced the structures in this region as too much of the structure, in particular the hanging-wall cutoffs of many faults, have been eroded. Rather, we can more effectively constrain the minimum shortening that is required to produce these structures (Fig. 12). In this assessment, two structures require especially large amounts of shortening: the Beichuan fault, which brings Precambrian rocks to the surface above Paleozoic rocks, and the frontal klippen, which place Paleozoic rocks above the Triassic section. To estimate the minimum shortening, we connect these two systems, allowing the same shortening to produce both structures. This is consistent with the interpretation of Chen and Wilson (1996). Alternatively, if the klippen root into the Wenchuan fault or another fault to the hinterland, the amount of shortening along the section must be much higher, by nearly a factor of 2, because two separate thrust systems, each with large displacements,

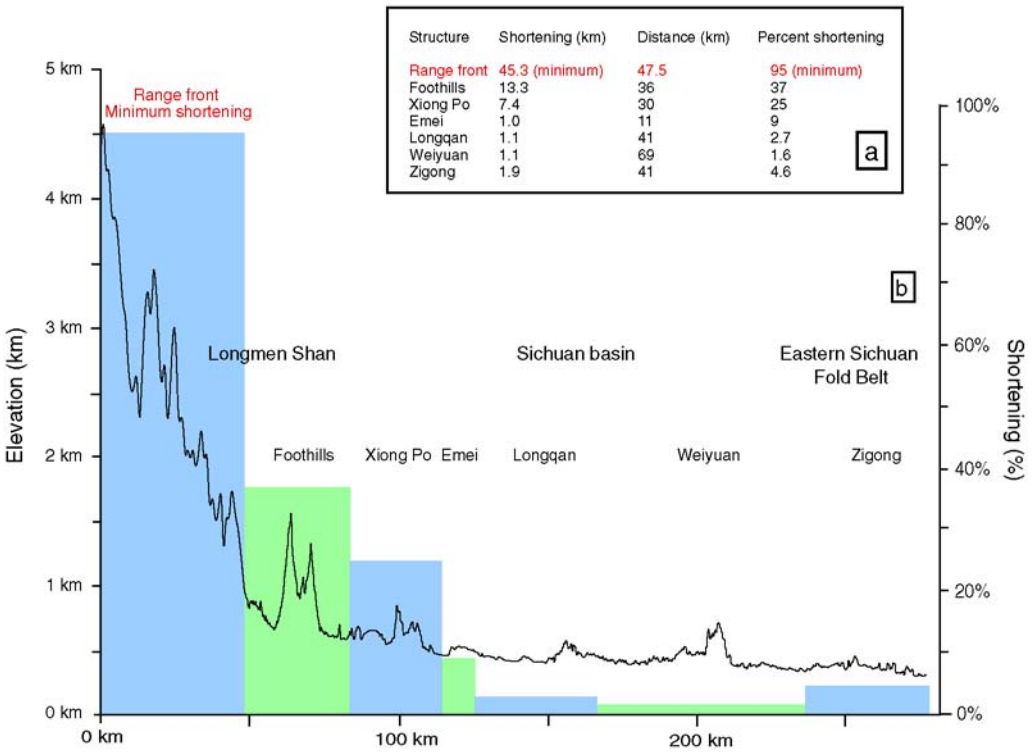

Figure 11. Shortening versus elevation, extending from the Sichuan basin into the Longmen Shan. Measurements from the foothills through the Zigong structure are made across cross sections D-D' and E-E' and are taken from Hubbard and Shaw (2009); left-most shortening measurement is from cross section C-C' (shortening solution is shown in Fig. 12). Note that the shortening and topography correlate extending into the high topography of the Longmen Shan. The color version of this figure is available only in the electronic edition.

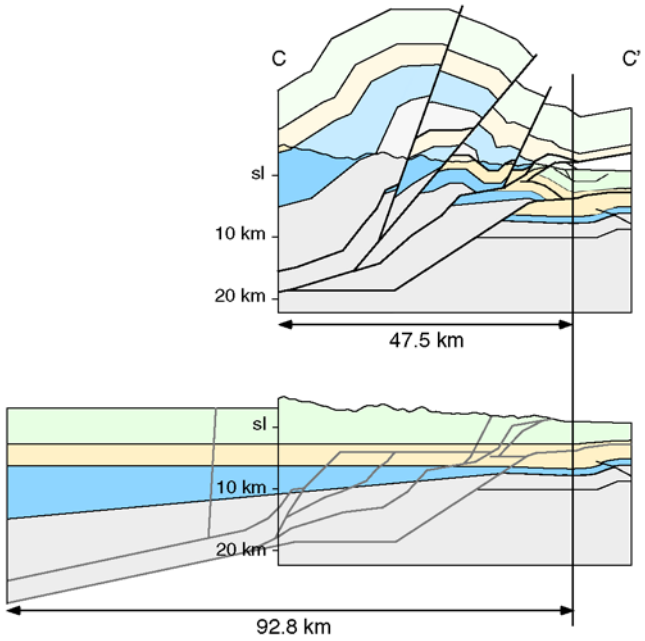

Figure 12. Minimum shortening solution for cross section C-C'. (a) Current deformed geometry; (b) Retrodeformed cross section. We measure a minimum of 45.3 km of shortening across this cross section, for a total percent shortening of $45.3/47.5 = 95\%$ shortening. Shades are the same as in the cross section in Figure 2. The color version of this figure is available only in the electronic edition.

are required to explain the structural observations. We also observe measurable shortening along the range front fault, the frontal faults, and the second splay of the Beichuan fault that exists along this cross section. We resolve no significant shortening on the Wenchuan fault, based on the mapped geometries and the fault and its cutoff relationships. The activity of this fault is unclear: Burchfiel *et al.* (1995) identified active dextral slip, while Densmore *et al.* (2007) found no unambiguous evidence for Quaternary displacement in their field studies.

Our assessment indicates that at least 45.3 km of shortening has been required over a distance of 47.5 km, or a minimum of 95% shortening. This indicates that shortening continues to increase westward into the higher ranges of the Longmen Shan, where the elevation reaches up to 4.5 km (Fig. 11). Collectively, these measurements establish that upper-crustal shortening correlates closely with present-day topography. Low magnitudes of shortening in the foreland are consistent with the gentle topography of the basin. In contrast, shortening increases substantially toward the range front and into the high peaks region of the Longmen Shan.

The shortening that we document likely represents the total sum of the contractional deformation in the basin and the range front. As we discussed, this deformation likely includes folding and faulting that occurred in both the Mesozoic (largely Triassic) and Cenozoic. Unfortunately, we cannot readily distinguish these different components of deformation, because we lack Cenozoic strata throughout most of the basin and range front. Nevertheless, in areas where we have seismic reflection data we observe that the magnitudes of Triassic shortening are modest; these structures are generally reactivated by somewhat higher amounts of Tertiary deformation. In the case of the Zhongba fold, for example, the total structural relief of the fold includes 400 m of Triassic uplift and 1100 m of post early Cretaceous uplift (Fig. 10). Given that the magnitudes of both Tertiary and Mesozoic deformation seem to increase into the ranges, this implies that the general patterns of low shortening in the basin and high shortening in the range front occurred in both the Mesozoic and Cenozoic fold belts. Furthermore, a basic plot of structural relief versus topography through the Sichuan basin and into the Longmen Shan (Fig. 13) shows that the structural relief far exceeds the total required to produce the current topography. Thus, we conclude that the topography in the basin and range front was produced by upper-crustal shortening, with a significant component of the shortening having occurred in the Tertiary. We consider the Wenchuan earthquake to be an active manifestation of this ongoing process.

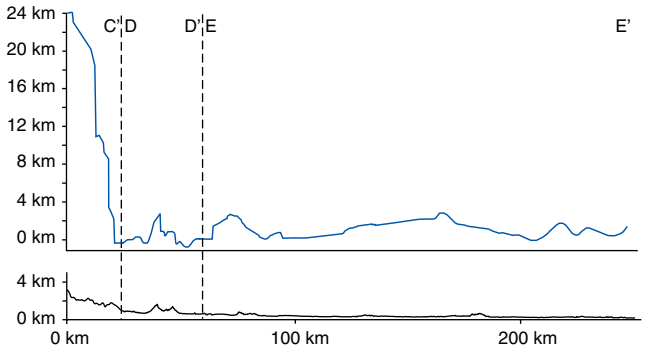

Figure 13. Structural relief versus topography for the cross sections C-C'-D-D'-E-E'. Structural relief for the section C-C' is derived from the top Paleozoic horizon of the minimum shortening solution (Fig. 12), while that along sections D-D' and E-E' is taken from a mid-Jurassic layer. The structural relief increases dramatically as the topography increases along cross section C-C', far exceeding the amount needed to produce the topography visible today. The structural relief along the northwestern half of line C-C' is not shown. This is because it is poorly constrained, as neither the Wenchuan fault nor other faults to the west of the line are considered in the minimum shortening model. The color version of this figure is available only in the electronic edition.

Insights from Critical Taper Wedge Mechanics

Given our assessment that upper-crustal shortening plays an important role in developing the topography of the Longmen Shan, we seek to explore if critical taper wedge mechanics, an established theory that describes the development of fold-and-thrust belts, can be successfully applied to model this deformation. This theory has been successfully applied to explain the geometries and mechanics of conventional orogenic and passive margin fold-and-thrust belts throughout the world. Critical-taper wedge mechanics theory explains the first-order geometry of fold-and-thrust belts as a function of the internal strength of the wedge of deforming material and the strength of the basal detachment on which the wedge slides (Davis *et al.*, 1983; Dahlen *et al.*, 1984). The analogy of a bulldozer pushing a pile of snow or sand is often used to illustrate the first-order mechanics (Fig. 14). Once the critical taper is reached, the wedge grows self-similarly, and internal deformation of the wedge maintains the taper. The taper of a specific wedge system is determined by the strength of the basal detachment relative to the internal strength of the wedge.

The Longmen Shan clearly involves important components of oblique-slip faulting that cannot be addressed by the critical taper models. While we do not seek to minimize the importance of oblique-slip faulting in the mountain belt, we suggest that the correlation between shortening and topography, the presence of active thrust faults throughout the fold belt, and the basic wedge-shaped geometry of the system indicate that aspects of the Longmen Shan may be effectively explained by critical taper models. Moreover, we suggest that the fold belt is at or near a state of critical taper because the deformation has propagated far out into the basin, implying that it has achieved critical taper in the range front. Small earthquakes near the Longquan anticline (Burchfiel *et al.*, 2008), within the Sichuan basin, indicate that this frontal portion of the wedge is active. Combined with fault activity

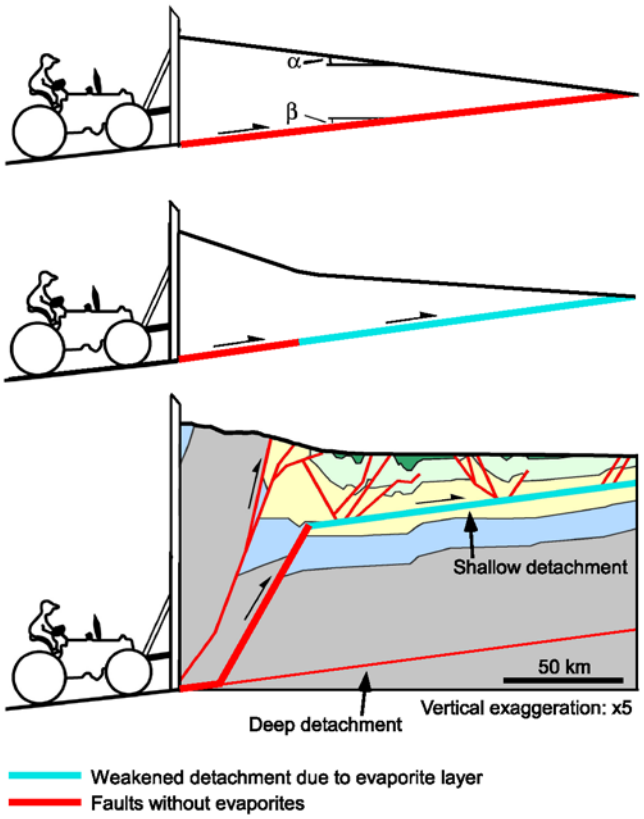

Figure 14. Conceptual models of (a) simple single-taper critical taper wedge and (b) double-taper critical taper wedge. (c) Cross section of the Sichuan basin and eastern Longmen Shan with thickened faults indicating the basal detachment. Weakened detachment due to evaporite layer and faults without evaporites are distinguished. Topography in (c) is the mean swath topography from Figure 15. The shades of the units are the same as in the cross section in Figure 2. Two wedge zones are defined here: the Sichuan basin, which has a shallow, weak detachment and a shallow surface slope, and the frontal Longmen Shan, which has a strong basal detachment and a steep surface slope. The color version of this figure is available only in the electronic edition.

documented in the Wenchuan earthquake, this suggests that both the foreland and hinterland portions of the fold belt are tectonically active.

Thus, we seek to explore if these critical taper models can explain the basic geometry of the mountain belt, including its topography, based on reasonable values of fault and wedge strength. In fact, the Longmen Shan displays two distinctive wedge geometries that we suggest reflect underlying fault properties and influence the rates of deformation across the fold belt. The topographic slope in the basin is very low, dipping approximately 0.1° to the southeast (Fig. 15). Moreover, the primary basal detachment for the active structures in the basin lies at a depth of about 4 km and dips very gently to the northwest (1.5°). Combined, these slopes indicate that the shape (or taper) of the fold-and-thrust belt in the basin is very narrow, consistent with either strong rocks within the wedge and/or a weak basal detachment. In contrast, the topographic gradient is steeper in the Longmen Shan, implying that the wedge taper is greater.

To explore this possible relation between the geometry and topography of the fold-and-thrust belt and its strength, we have defined a range of critical taper wedge models of the Longmen Shan range front and the western Sichuan basin, using the formulation of Dahlen *et al.* (1984) as implemented in Bilotti and Shaw (2005). These models incorporate detachment geometries derived from our seismic reflection data and geologic sections, and measures of wedge and detachment properties (e.g., density, fluid pressure, cohesive strength, and frictional coefficients) inferred from our understanding of the regional geology.

The taper of a subaerial wedge can be written following Dahlen (1990) as:

$$\alpha + \beta \approx \frac{\beta + \mu_b(1-\lambda_b) + S_b/\rho g H}{1 + 2(1-\lambda)[\frac{\sin(\phi)}{1-\sin\phi}] + C/\rho g H}, \qquad (1)$$

where α and β are the dips of the topography and the detachment in radians, respectively; $\mu = \tan(\phi)$ and μ_b are the coefficients of friction of the wedge and basal detachment, respectively, where ϕ is the friction angle; λ and λ_b are the Hubbert–Rubey fluid-pressure ratios for the wedge and the basal detachment, respectively (Hubbert and Rubey, 1959); C and S_b are the cohesive strengths of the wedge and the basal detachment, respectively; ρ is the density of the wedge; and H is the thickness of the wedge (vertical distance from the detachment to the topographic surface).

Table 1 gives the parameter ranges that we explored for our critical taper wedge model. Within the Sichuan basin, given the assumption that the wedge is hydrostatic and considering reasonable ranges of other basic parameters, we conclude that the basal coefficient of friction must be very low, < 0.25. Note that if the wedge had higher basal fluid pressures, then the estimated basal frictions would be even lower. On the other hand, higher internal fluid pressures would indicate higher basal frictions. In any case, the absolute strength of the basal detachment, as defined by Suppe (2007), must be very low. These low values of basal friction are consistent with values measured in Taiwan (0.04–0.1, Suppe, 2007).

In contrast, the range front topography is much steeper, implying a greater effective strength to the underlying basal detachment. The dip of the basal detachment under the Longmen Shan, however, cannot be precisely constrained given the available geologic and seismologic observations. Thus, we must consider a wider range of possible detachment dips. For a low detachment dip of 1.5° (the same as within the Sichuan basin), the basal friction coefficient must range from 0.14–0.61, which is stronger than that inferred for the basin given the steeper topographic gradient, but still weak compared with Byerlee's law (0.6–0.85; Byerlee, 1978). Increasing the detachment dip would yield higher basal friction values. Detachment dips of up to about 17°, which is close to the dip of the ramp connecting the upper detachment

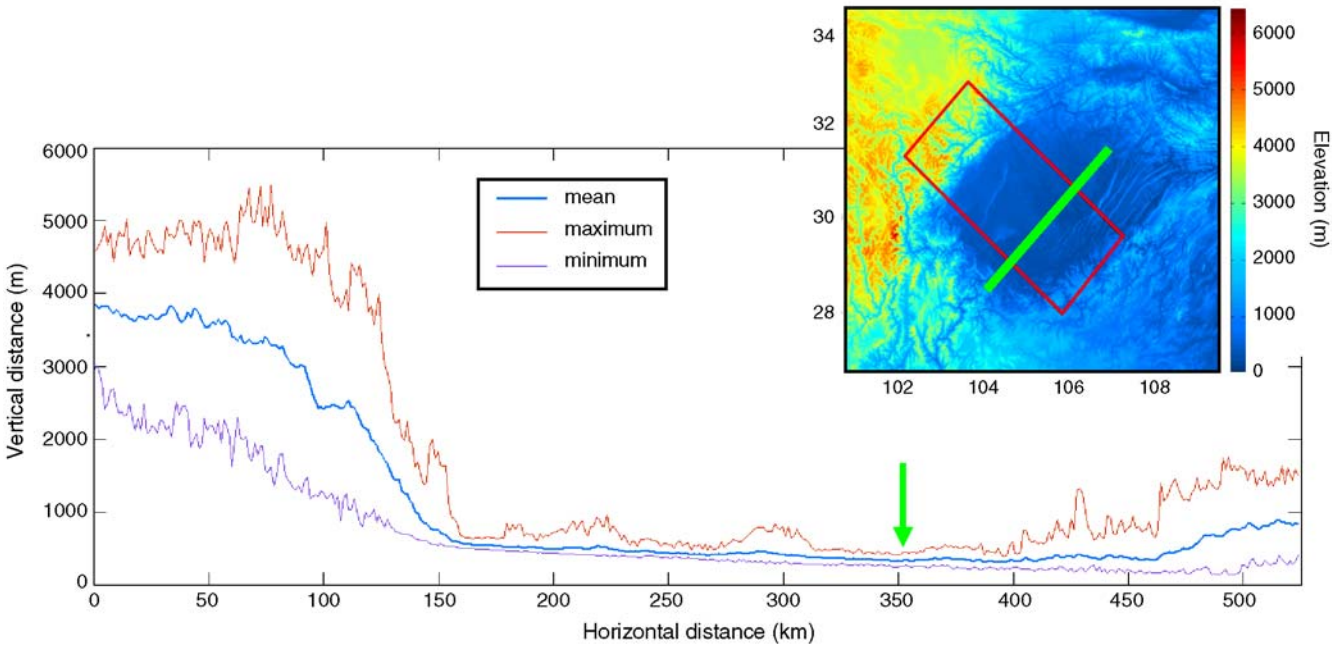

Figure 15. Swath profile (northwest to southeast) of the Longmen Shan and Sichuan basin. Mean, maximum, and minimum elevations are shown. The location of the profile is given on the inset map. The thick line on the map and arrow on the profile indicate the southeastern limit of the wedge, as defined by the location where the mean topography diverges from a shallow constant slope of ~0.068°. The color version of this figure is available only in the electronic edition.

beneath the Sichuan basin with the lower detachment beneath the Longmen Shan, would still yield basal friction values consistent with Byerlee's law. However, achieving this dip requires the coefficient of friction within the wedge to be lower than that at the base ($\mu = 0.72 < \mu_b = 0.9$), which is both unlikely and invalidates the critical taper equation used (equation 1 is the small-angle approximation of the full equation and is only valid as long as $\mu_b(1 - \lambda_b) \ll \mu(1 - \lambda)$; Dahlen, 1990). In addition, this detachment dip is far higher than those defined for most other fold belts (e.g., Barbados: $\beta = 2°$, Dahlen, 1990; Taiwan: $\beta = 6°$, Davis *et al.*, 1983; Niger Delta: $\beta = 1.2$–$2.2°$, Bilotti and Shaw, 2005). Thus, we feel that a shallow detachment dip, closer to 1.5°, is more likely if the Longmen Shan is behaving as a critical taper wedge. Finally, we suggest that this inferred deep detachment may extend out into the Sichuan basin, and link to the Weiyuan anticline (regional cross section in Fig. 4). The Weiyuan fold is clearly distinct from the

Table 1
Parameters Used in Critical Taper Wedge Modeling

Parameter	Value		Method of Determination
	Sichuan	Longmen Shan	
Surface slope α	0.068°	2.1°	Measured from swath topography
Detachment dip β	1.5°	0–17°	Sichuan: measured from seismic section; Longmen Shan: see discussion in text
Thickness H	4 km	19 km	Sichuan: measured from seismic section; Longmen Shan: inferred from geologic cross section
Density ρ	2700 kg/m^3	–	Average crustal value
Fluid-pressure ratio λ	$P_f/\rho gH \approx \rho_w gH/\rho gH = \rho_w/\rho = 1/2.7 \approx 0.370$	–	Hydrostatic approximation (assumes no overpressure)
Basal fluid-pressure ratio λ_b	$\rho_w/\rho = 1/2.7 \approx 0.370$	–	Same as for λ
Wedge cohesion C	0–20 MPa	–	Hoshino *et al.* (1972); Bilotti and Shaw (2005)
Basal cohesion S_b	0–5 MPa	–	Hoshino *et al.* (1972); Bilotti and Shaw (2005)
Internal coefficient of friction μ	0.5–1.4	–	Suppe (1984)
Basal coefficient of friction μ_b	0–0.25	0.14–0.95	Sichuan: Modeled result given other constraints; Longmen Shan: lower bound–modeled result; upper bound–Byerlee

other structures that we have documented in the basin above the shallow basin detachment, because the fold extends to at least 7 km depth, at the limit of our seismic images.

In order to determine the cause of the different implied strengths for the basal detachments beneath the basin and the range front, we explore the nature of the rocks that host the basal detachments in these two areas. Based on our seismic reflection data and well control, we observe that the basal detachment for most structures in the basin is localized within a Triassic evaporite sequence (Fig. 16). The evaporites

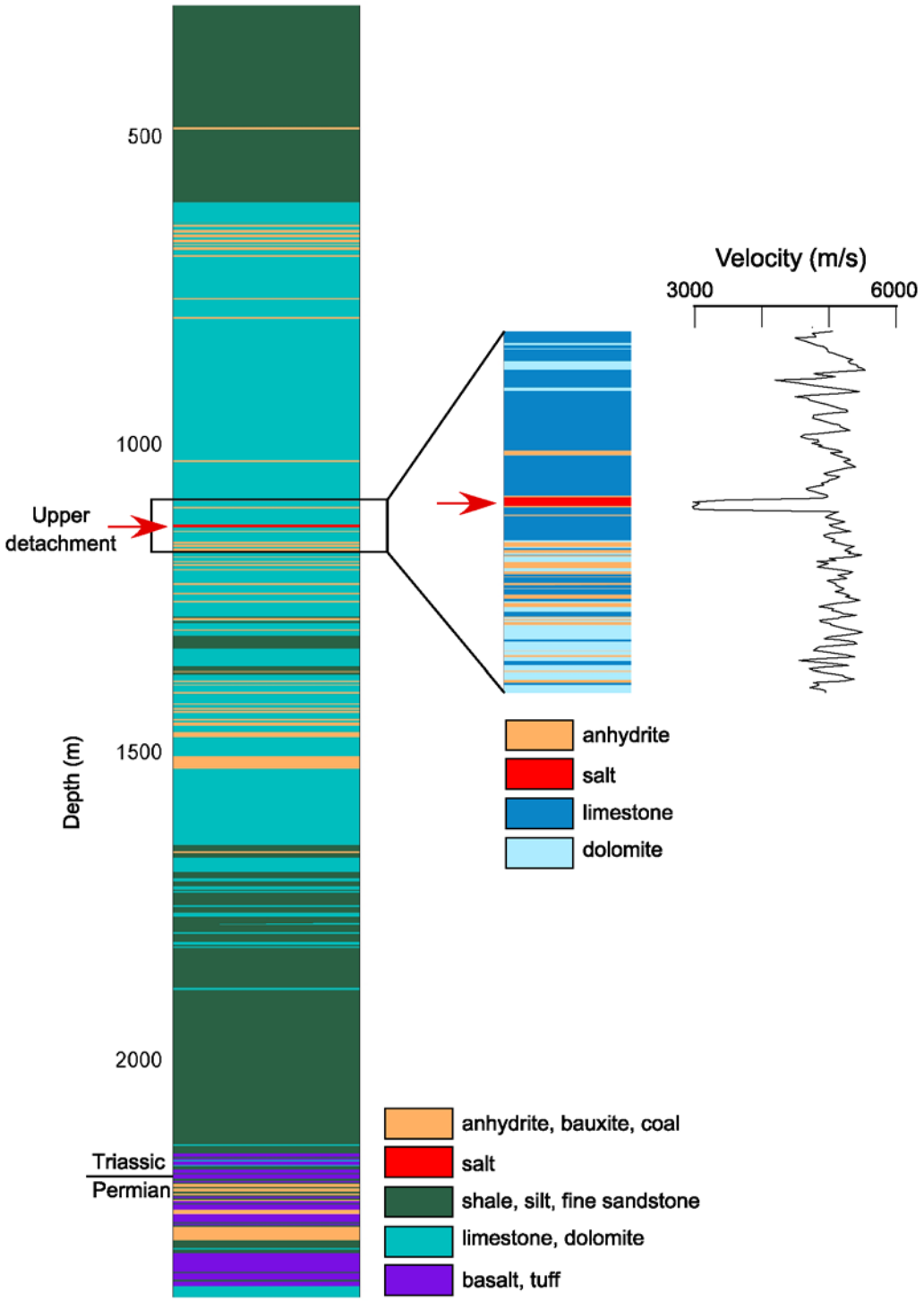

Figure 16. Well showing the rock types and acoustic (*P* wave) velocities down to ~2.4 km. For the location of the well, see Figures 1 and 3. Note the presence of a salt layer at ~1.1–1.2 km, coincident with a strong decrease in velocity. The depth of this layer matches the depth of the detachment visible in the seismic data. The color version of this figure is available only in the electronic edition.

likely impose a very effective weak basal friction on the fold-and-thrust belt, consistent with the predictions of the critical taper models. This weak basal detachment produces the very narrow wedge shape and gentle topographic slope in the basin (Figs. 17, 18). This weak detachment has also enabled thrust sheets to propagate very far to the east into the center of the basin, because only small amounts of shortening are required to achieve the critical taper. In contrast, the front ranges of the Longmen Shan exhibit steep topographic slopes, consistent with the predicted increase in the strength of the basal detachment. The geology of the range front indicates that the basal detachment must step down beneath the range front (Figs. 2, 6, 7). Specifically, the Triassic strata that contain the detachment in the basin are folded and exposed at the surface in the range front, requiring that the thrust faults in the range front must sole to a deeper stratigraphic level. The base of the thrusts in the range front must also be deeper than in the basin, given the depth of faulting in the Wenchuan earthquake (> 16 km). This implies that a basal detachment in the range front would lie at midcrustal levels in Precambrian metasedimentary or igneous rocks, based on the observation that the Beichuan fault carries Precambrian intrusive rocks to the surface. This change in detachment depth occurs along the change in topographic slope (Fig. 6). Thus, we suggest that the change in strength of the basal detachment causes the change in the wedge shape and topographic slope (Figs. 17, 18). This, in turn, implies a marked increase in the amount of internal deformation that is required within the range front versus the basin in order to achieve the critical taper. This predicted increase in shortening moving from the basin to the range front has been documented in our previous discussion.

This analysis demonstrates that the fold-and-thrust belt of the western Sichuan basin and Longmen Shan can be

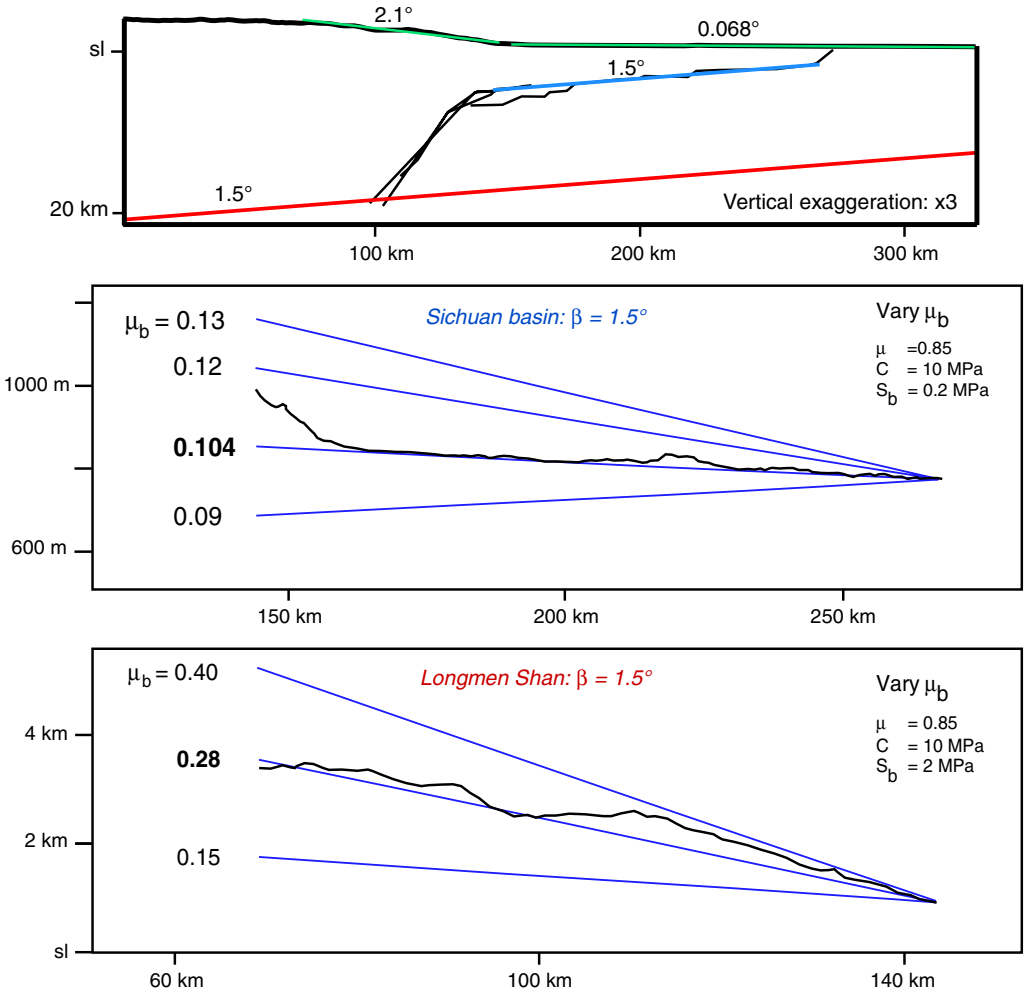

Figure 17. Modeled topographic profiles showing the effect of varying the coefficient of friction of the basal detachment, μ_b, for the upper detachment underlying the Sichuan basin and the lower detachment underlying the Longmen Shan. The upper cross section shows the mapped geometry of the upper detachment and the ramp. The values of μ, C, and S_b are fixed to reasonable numbers; to see the effects of varying these parameters, see Figure 18. Note that the coefficient of friction of the detachment under the Sichuan basin must be very low to produce the observed topography, while that under the Longmen Shan must be higher. The upper 1.5° line in the cross section indicates the location of the upper detachment, while the lower 1.5° line indicates the location of the lower detachment. The color version of this figure is available only in the electronic edition.

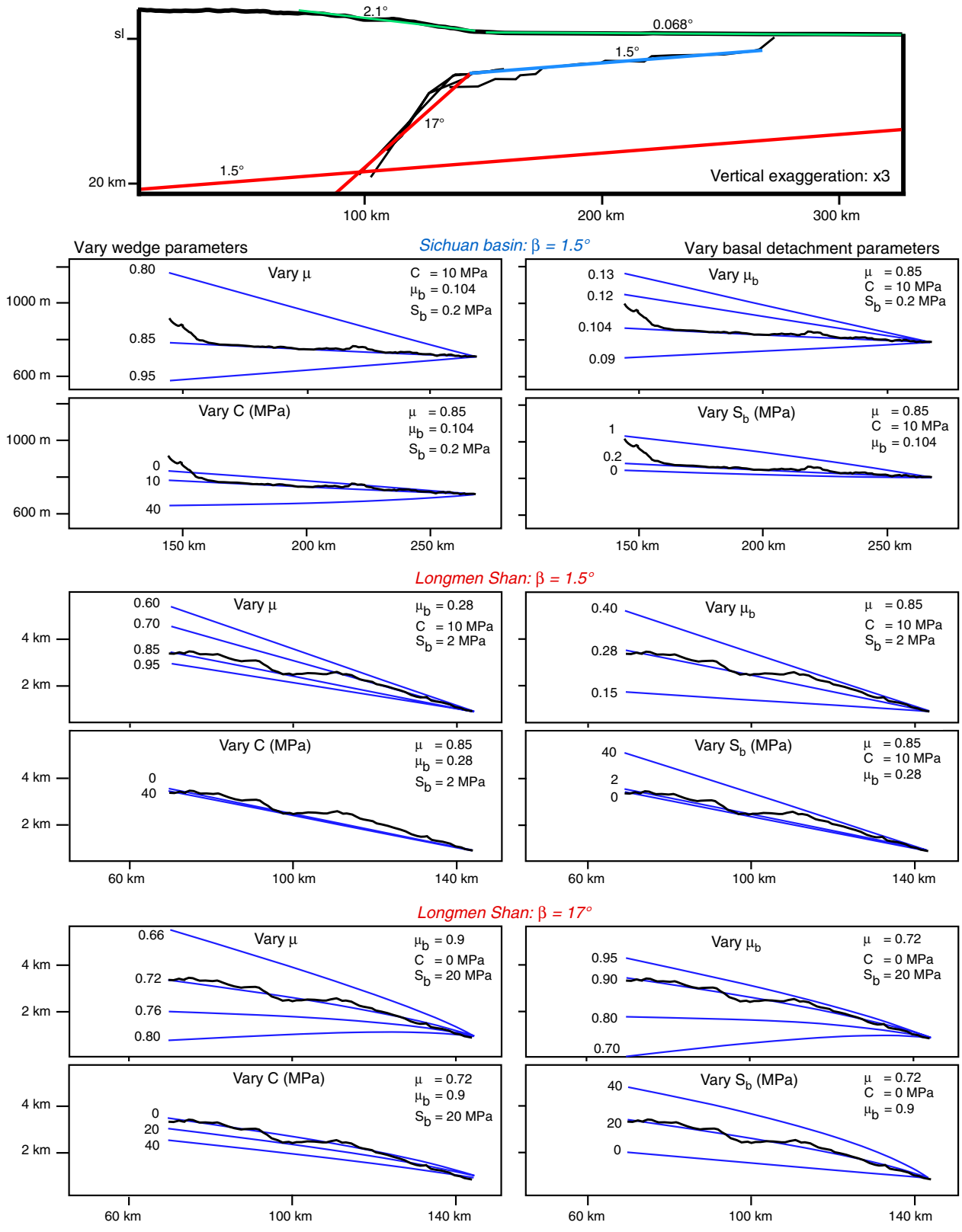

Figure 18. Modeled topographic profiles showing the effects of varying the wedge and basal detachment parameters: the coefficient of friction of the wedge and the basal detachment μ and μ_b, and the cohesion of the wedge and the basal detachment, C, and S_b, for the upper detachment underlying the Sichuan basin, the lower detachment underlying the Longmen Shan, and a ramp dipping 17° extending from the upper detachment to the lower one. The upper cross section shows the mapped geometry of the upper detachment and the ramp. The upper 1.5° line in the cross section indicates the location of the upper detachment, while the lower 1.5° line and the 17° line indicate the locations of the lower detachment and the ramp, respectively. The color version of this figure is available only in the electronic edition.

modeled as a critical taper wedge with reasonable rock and fault strength parameters. The low taper in the Sichuan basin is consistent with a low basal friction, which is to be expected given the observation that the detachment lies within a Triassic evaporite sequence. The steeper topography of the range front can similarly be modeled as a critical taper wedge yielding higher, but still reasonable, values of basal friction. Thus, while the topographic gradient of the Longmen Shan is clearly very steep, it can nevertheless be modeled as a critical taper wedge using values of basal fault strength that are indeed considerably less than laboratory measurements of static fault friction. We suggest that this result further supports our conclusion, based on our correlation of upper-crustal shortening and topography, that the Longmen Shan mountain range does not require any extraordinary mechanism of uplift, but rather can be explained by crustal shortening.

This critical taper analysis also provides insights into another noteworthy aspect of the Wenchuan earthquake, namely that the rupture occurred on faults that are more than 200 km west of the toe of the fold-and-thrust belt. Traditionally, most fold-and-thrust belts are thought to develop by break-forward propagation of thrust sheets, implying that the youngest, and most active, thrust sheets lie in the toe of the fold-and-thrust belt. Thus, several authors (e.g., Liu-Zeng *et al.*, 2009) have described the Wenchuan earthquake as an out-of-sequence event. However, our analysis demonstrates that over geologic timescales, the amount of shortening in the toe of the fold-and-thrust belt (1.6–2.7%) is much less than that observed in the range front (>95%). This is consistent with the inference, based on critical taper analysis, that the basal detachment beneath the basin is very weak. Thus, only small amounts of shortening are required to achieve critical taper. In contrast, when the detachment steps back into the range front, it drops substantially below the evaporite section, and thus presumably has greater strength. This is reflected in the steeper topography of the range front, which requires much more internal shortening within the fold-and-thrust belt to achieve the critical taper. Furthermore, higher rates of erosion in the range front relative to the basin would further increase the required shortening rates of the Longmen Shan to maintain the critical taper. Thus, if earthquake activity reflects geologic shortening rates, it implies that the moment release rate from earthquakes in the range front would be much larger than that in the basin. In other words, while the Wenchuan event was out-of-sequence in a geometric sense, it likely represents the more typical location for large earthquakes in the fold-and-thrust belt, and events in the basin might be very rare. Indeed, given the weakness and shallowness of the active detachment level in the basin, it is unclear whether these faults can support significant enough stresses to generate large earthquakes.

Discussion

We suggest that the correlation between topography, structural relief, and shortening in the Sichuan basin and Longmen Shan indicates that upper-crustal shortening is the primary process driving the development of steep topography along the range front. This seems to obviate the need for lower-crustal flow and inflation to produce and maintain the Longmen Shan range front. The inflation mechanism was initially proposed to explain the topography of the range front and plateau in the absence of significant crustal shortening. Thus, our documentation of significant amounts of crustal shortening that are spatially correlated with, and sufficient in magnitude to explain, the topography of the range front argues that the mountain belt has developed by the classic mechanism of upper-crustal faulting and folding (e.g., Chapple, 1978; Boyer and Elliott, 1982; Matte, 1986; Platt, 1986; Alavi, 1993). Moreover, we argue that if lower-crustal flow occurs in the interior of the mountain belt beneath the Tibetan Plateau, it must somehow be directly coupled to upper-crustal deformation in the range front.

The inflation model of the Longmen Shan was largely derived from the apparent paradox of low geodetic and geologic shortening rates and lack of a traditional foreland basin together with high relief. Next, we address how these observations might also be consistent with our results.

Low shortening rates do not mean low shortening. Indeed, we show that the shortening recorded in the rocks far exceeds that required to build the current relief, based on current understanding of erosion rates. Shortening rates of 3 mm/yr (as measured by geodesy) require a spatially averaged erosion rate of 1.2 mm/yr across the range to maintain steady-state (assuming shortening on a 20-km-deep detachment accommodated over a width of 50 km). This erosion rate is consistent with fluvial incision rates of 0.5–3 mm/yr (Kirby, 2001; Kirby *et al.*, 2003) and thermochronological denudation rates of 0.5–2 mm/yr (Kirby *et al.*, 2002; Godard, Pik *et al.*, 2009) in the Longmen Shan. Furthermore, today's shortening rates may be lower than they were in the past, and erosion simply has not had enough time to significantly reduce the relief. In this context, isostatic rebound could be extending the lifetime of the mountain range. More detailed models showing the stability of high-gradient margins in the absence of significant shortening can be found in Godard, Cattin *et al.* (2009). Finally, the interseismic shortening rates measured geodetically before the Wenchuan earthquake could be underestimating the long-term shortening rates, given that they were sampling a period in advance of a massive earthquake (e.g., Chéry and Vernant, 2006). Factoring in the coseismic shortening of 3–9 m in the Wenchuan event (Lin *et al.*, 2009; Xu *et al.*, 2009), shortening rates would be substantially larger than 3 mm/yr even if such earthquakes were relatively infrequent in the range front.

As we discussed previously, some of the shortening recorded in our sections was produced prior to the development of the current relief. As the Sichuan basin does not record significant sedimentary deposits younger than Jurassic, we cannot fully distinguish the Mesozoic from Cenozoic components of this deformation. Nevertheless, our analysis

suggests that, in at least some cases, Cenozoic structures in the range front reactivate older Mesozoic features, and the magnitude of Cenozoic deformation is substantial (Fig. 10). Combined with our previous assessment that the documented total shortening is far greater than needed to build the topography of the ranges, we suggest that Cenozoic deformation plays a direct role in maintaining the present-day topography of the range front.

In addition, we suggest that the growth of the mountain belt due to shortening is not incompatible with the lack of a typical foreland basin. While it is true that there is no deep, localized depression just to the southeast of the Longmen Shan, a foreland basin does exist in the form of the slight (1.5°) dip of the western half of the basin toward the mountain range. In addition, Cenozoic sediments are deposited in thin patches near the range front. We also note that the Sichuan basin is not a depositional basin; instead, sediments shed off of the mountain range are carried through the basin and out to south China through a network of rivers (e.g., Clark *et al.*, 2004). Thus, there is no sediment loading to contribute to the formation of a deep foreland basin. Finally, the basin and lithosphere that underlie it are likely strong and thick, based on tomography that images a high-velocity root beneath the basin that is up to 200 km deep (Li *et al.*, 2006). This suggests that the flexural strength of the basin and underlying lithosphere is very high. This apparent strength, together with the small areal extent of the basin and the fact that it is bounded by fold-and-thrust belts on all four sides, likely disfavors the development of a traditional foreland basin.

Implications for Regional Earthquake Hazards

The Longmen Shan and Sichuan basin systems are zones of active reverse and oblique-slip faulting (Densmore *et al.*, 2007; Liu-Zeng *et al.*, 2009; Xu *et al.*, 2009; Li *et al.*, 2010) and contain a number of faults that may be capable of generating large earthquakes. These include along-strike sections of faults that ruptured in the Wenchuan earthquake, the Wenchuan and Range Front faults, and possibly structures within the basin. As in the Wenchuan rupture, future large earthquakes could involve multiple subparallel faults, bridging lateral segment boundaries, including stepovers.

We suggest that the rates of deformation in the system, and hence hazards, vary as a function of basal detachment strength and erosion, and can be quantified through our critical taper wedge mechanics analysis. The implications for regional earthquake hazards based on this model do not rely on the parameters used to model the wedge, but instead on the basic conclusion that higher and lower amounts of shortening in the ranges and basin, respectively, are required to build their wedge tapers. Moreover, higher erosion rates in the ranges imply that additional shortening is required in this area to maintain the taper.

The plausible locations of earthquakes to a first order can be defined by the lateral extent of the wedge within the Sichuan basin. Beyond the toe of the wedge, we do not expect the system to source earthquakes. We can identify the approximate location of the toe by fitting a linear trend to the mean swath topography of the Sichuan basin and determining where the topography diverges from this slope. This suggests that the toe of the fold belt is located about 200 km to the east of the western margin of the basin and that all regions to the west of this location are potentially active parts of the fold belt (Fig. 15). However, it seems unlikely that those faults that rise from the very weak, very shallow (<5 km) detachment within the Sichuan basin are capable of storing sufficient amounts of elastic strain energy to generate large earthquakes. Indeed, there appear to be no historic records of large earthquakes that have occurred in the basin above these shallow detachment systems. In addition, calculations of Coulomb stress changes suggest that the Wenchuan earthquake lowered the stress on the northern part of this fault system, decreasing the likelihood of a rupture near Chengdu (Parsons *et al.*, 2008). Collectively, these observations and calculations suggest that large earthquakes are unlikely to nucleate in the basin above the shallow detachment.

Rather, the critical taper wedge model implies that shortening rates must be much higher in the range front; given the greater depths of these faults, they seem much more likely than their counterparts in the basin to generate large earthquakes. In addition to the greater depth and inferred strength of the faults in the range front, higher erosion rates in this area likely also promote greater fault activity. As erosion removes material from the range front and decreases its topographic slope, the wedge must deform internally in order to maintain its taper. Thus, it must accommodate additional shortening in the interior of the fold belt. The location of the Wenchuan earthquake, occurring in the range front rather than the basin, may reflect this effect. The Longmen Shan experiences much higher erosion rates than the Sichuan basin, due to the difference in slope (~5–80 times higher: 0.5–2 mm/yr in the Longmen Shan, according to Godard, Pik *et al.* [2009] and Kirby *et al.* [2002], compared with 0.025–0.1 mm/yr in the Sichuan basin, from 1–4 km exhumation over 40 m.y., Richardson *et al.* [2008]). Thus, the range front must accommodate much more shortening than the Sichuan basin, producing much higher rates of faulting and large earthquakes. In the first part of this paper, we measured the shortening recorded in the upper crust and demonstrated that it was, in fact, much higher (perhaps by 35–60 times) than in the basin (minimum of 95% shortening in the range front compared with 1.6–2.7% across the Longquan and Weiyuan structures). This analysis suggests that the frontal part of the Longmen Shan is at the greatest risk of large earthquakes, as demonstrated by the Wenchuan rupture. Average recurrence intervals of 2,000–10,000 years (Burchfiel *et al.*, 2008) and 3000–6000 years (Li *et al.*, 2008) have been estimated for major earthquakes on the Beichuan fault. While it is unlikely that the Beichuan fault will rupture again in the near future, other faults in the system, including the Range Front thrust and the northern frontal

faults, as well as the faults that extend to the northeast and southwest of the rupture, could still source large earthquakes.

Conclusions

The Wenchuan earthquake demonstrates the ability of thrust fault earthquakes to involve multiple thrust splays and rupture across significant lateral segment boundaries. This illustrates that comprehensive assessments of earthquake hazard in this region and in other fold-and-thrust belts around the world must consider the possibility of very large ruptures occurring along multiple faults. For these very large but infrequent earthquake scenarios, historical earthquake catalogs and geodetic data may not be sufficient to identify and characterize hazards. Instead, it may be necessary to combine these data with subsurface and surface mapping to define the geometries and activities of faults in order to fully document hazards. Measurements of long-term shortening recorded in the upper crust along faults and folds, combined with critical taper wedge mechanics models, can provide a way to better understand the earthquake hazard in a mountain belt.

Data and Resources

The seismic reflection database was provided courtesy of Texaco and the China National Petroleum Company and is proprietary.

Earthquake focal mechanisms and preferred nodal planes were taken from the U.S. Geological Survey's National Earthquake Information Center and the Global Moment Tensor Project database (searched using http://neic.usgs.gov/neis/epic/epic.html and www.globalcmt.org/CMTsearch.html; last accessed on 8 October 2009).

Acknowledgments

We are indebted to Chris Connors (Washington and Lee University) and Greg Slutz (Chevron) for their expertise and insights into the geology of the Longmen Shan. We also thank Li Yiquan (Nanjing University); Li Benliang (PetroChina); John Suppe (National Taiwan University), and Dengfa He (China University of Geosciences) for their helpful discussions.

References

Alavi, M. (1993). Tectonics of the Zagros orogenic belt of Iran: New data and interpretations, *Tectonophysics* **229,** 221–238.

Baljinnyam, I., A. Bayasgalan, B. A. Borisov, A. Cisternas, M. G. Dem'yanovich, L. Ganbaatar, V. M. Kochetkov, R. A. Kurushin, P. Molnar, H. Philip, and Yu. Ya. Vashchilov (1993). Ruptures of major earthquakes and active deformation in Mongolia and its surroundings, *Mem. Geol. Soc. Am.* **181**.

Bilotti, F., and J. H. Shaw (2005). Deepwater Niger Delta fold-and-thrust belt modeled as a critical-taper wedge: The influence of elevated basal fluid pressure on structural styles, *AAPG Bull.* **89,** 1475–1491.

Bird, P. (1991). Lateral extrusion of lower crust from under high topography, in the isostatic limit, *J. Geophys. Res.* **96,** 10,275–10,286.

Bowman, D., G. King, and P. Tapponnier (2003). Slip partitioning by elastoplastic propagation of oblique slip at depth, *Science* **300,** 1121–1123.

Boyer, S. E., and D. Elliott (1982). Thrust systems, *AAPG Bull.* **66,** 1196–1230.

Burchfiel, B. C. (2004). 2003 Presidential address: New technology, new geological challenges, *GSA Today (Geological Society of America)* **14,** 4–9.

Burchfiel, B. C., Z. Chen, Y. Liu, and L. H. Royden (1995). Tectonics of the Longmen Shan and adjacent regions, central China, *Int. Geol. Rev.* **37,** 661–735.

Burchfiel, B. C., L. H. Royden, R. D. van der Hilst, B. H. Hager, Z. Chen, R. W. King, C. Li, J. Lü, H. Yao, and E. Kirby (2008). A geological and geophysical context for the Wenchuan earthquake of 12 May 2008, Sichuan, People's Republic of China, *GSA Today (Geological Society of America)* **18,** 4–11.

Byerlee, J. (1978). Friction of rocks, *Pure Appl. Geophys.* **116,** 615–626.

Chapple, M. (1978). Mechanics of thin-skinned fold-and-thrust belts, *Geol. Soc. Am. Bull.* **89,** 1189–1198.

Chen, S. F., and C. J. L. Wilson (1996). Emplacement of the Longmen Shan Thrust-Nappe Belt along the eastern margin of the Tibetan Plateau, *J. Struct. Geol.* **18,** 413–430.

Chen, S. F., C. J. L. Wilson, Q. D. Deng, X. L. Zhao, and Z. L. Luo (1994). Active faulting and block movement associated with large earthquakes in the Min Shan and Longmen Mountains, northeastern Tibetan Plateau, *J. Geophys. Res.* **99,** 24,025–24,038.

Chen, Z., B. C. Burchfiel, Y. Liu, R. W. King, L. H. Royden, W. Tang, E. Wang, J. Zhao, and X. Zhang (2000). Global Positioning System measurements from eastern Tibet and their implications for India/Eurasia intercontinental deformation, *J. Geophys. Res.* **105,** 16,215–16,227.

Chéry, J., and P. Vernant (2006). Lithospheric elasticity promotes episodic fault activity, *Earth Planet. Sci. Lett.* **243,** 211–217.

Clark, M. K., and L. H. Royden (2000). Topographic ooze: Building the eastern margin of Tibet by lower crustal flow, *Geology* **28,** 703–724.

Clark, M. K., J. W. M. Bush, and L. H. Royden (2005). Dynamic topography produced by lower crustal flow against rheological strength heterogeneities bordering the Tibetan Plateau, *Geophys. J. Int.* **162,** 575–590.

Clark, M. K., L. M. Schoenbohm, L. H. Royden, K. X. Whipple, B. C. Burchfiel, X. Zhang, W. Tang, E. Wang, and L. Chen (2004). Surface uplift, tectonics, and erosion of eastern Tibet from large-scale drainage patterns, *Tectonics* **23,** doi 10.1029/2002TC001402.

Cook, K. L., and L. H. Royden (2008). The role of crustal strength variations in shaping orogenic plateaus, with application to Tibet, *J. Geophys. Res.* **114,** doi 10.1029/2007JB005457.

Dahlen, F. A. (1990). Critical taper model of fold-and-thrust belts and accretionary wedges, *Annu. Rev. Earth Planet. Sci.* **18,** 55–99.

Dahlen, F. A., J. Suppe, and D. Davis (1984). Mechanics of fold-and-thrust belts and accretionary wedges: Cohesive Coulomb theory, *J. Geophys. Res.* **89,** 10,087–10,101.

Dahlstrom, C. D. A. (1969). Balanced cross sections, *Can. J. Earth Sci.* **6,** 743–757.

Davis, D., J. Suppe, and F. A. Dahlen (1983). Mechanics of fold-and-thrust belts and accretionary wedges, *J. Geophys. Res.* **88,** 1153–1172.

Densmore, A. L., M. A. Ellis, Y. Li, R. Zhou, G. S. Hancock, and N. Richardson (2007). Active tectonics of the Beichuan and Pengguan faults at the eastern margin of the Tibetan Plateau, *Tectonics* **26,** doi 10.1029/2006TC001987.

Duan, B., and D. D. Oglesby (2006). Heterogeneous fault stresses from previous earthquakes and the effect on dynamics of parallel strike-slip faults, *J. Geophys. Res.* **111,** doi 10.1029/2005JB004138.

Elliott, A. J., J. F. Dolan, and D. D. Oglesby (2009). Evidence from coseismic slip gradients for dynamic control on rupture propagation and arrest through stopovers, *J. Geophys. Res.* **114,** doi 10.1029/2008JB005969.

Gaudemer, Y., P. Tapponnier, B. Meyer, G. Peltzer, Shunmin Guo, Zhitai Chen, Huagung Dai, and I. Cifuentes (1995). Partitioning of crustal slip between linked, active faults in the eastern Qilian Shan, and evidence for a major seismic gap, the 'Tianzhu gap', on the western Haiyuan fault, Gansu (China), *Geophys. J. Int.* **120,** 599–645.

Godard, V., R. Cattin, and J. Lavé (2009). Erosional control on the dynamics of low-convergence rate continental plateau margins, *Geophys. J. Int.* **179,** 763–777.

Godard, V., R. Pik, J. Lavé, R. Cattin, B. Tibari, J. de Sigoyer, M. Pubellier, and J. Zhu (2009). Late Cenozoic evolution of the central Longmen Shan, eastern Tibet: Insight from (U-Th)/He thermochronometry, *Tectonics* **28,** doi 10.1029/2008TC002407.

Haeussler, P. J., D. P. Schwartz, T. E. Dawson, H. D. Stenner, J. J. Lienkaemper, B. Sherrod, F. R. Cinti, P. Montone, P. A. Craw, A. J. Crone, and S. F. Personius (2004). Surface rupture and slip distribution of the Denali and Totschunda faults in the 3 November 2002 *M* 7.9 earthquake, Alaska, *Bull. Seismol. Soc. Am.* **94,** S23–S52, doi 10.1785/0120040626.

Hoshino, K., K. Inami, S. Iwamura, H. Koide, and S. Mitsui (1972). *Mechanical properties of Japanese Tertiary sedimentary rocks under high confining pressures*, Japanese Geological Survey Report, no. 244, 200 pp.

Huang, R., Z. Wang, S. Pei, and Y. Wang (2009). Crustal ductile flow and its contribution to tectonic stress in Southwest China, *Tectonophysics* **473,** 476–489.

Hubbard, J., and J. H. Shaw (2009). Uplift of the Longmen Shan and Tibetan plateau, and the 2008 Wenchuan ($M = 7.9$) earthquake, *Nature* **458,** 194–197.

Hubbert, M. K., and W. M. Rubey (1959). Role of fluid pressure in mechanics of overthrust faulting, *Geol. Soc. Am. Bull.* **70,** 115–166.

Ji, C., and G. Hayes (2008). Preliminary result of the May 12, 2008 M_w 7.9 eastern Sichuan, China earthquake, http://earthquake.usgs.gov/eqcenter/eqinthenews/2008/us2008ryan/finite_fault.php, last accessed October 13, 2009.

Jia, D., G. Q. Wei, Z. X. Chen, B. L. Li, Q. Zeng, and G. Yang (2006). Longmen Shan fold-thrust belt and its relation to the western Sichuan Basin in central China: New insights from hydrocarbon exploration, *AAPG Bull.* **90,** 1425–1447.

King, G., Y. Klinger, D. Bowman, and P. Tapponnier (2005). Slip-partitioned surface breaks for the M_w 7.8 2001 Kokoxili earthquake, China, *Bull. Seismol. Soc. Am.* **95,** 731–738.

Kirby, E. (2001). Structural, thermal and geomorphic evolution of the eastern margin of the Tibetan Plateau, *Ph.D. Thesis*, Massachusetts Institute of Technology, Cambridge.

Kirby, E., P. W. Reiners, M. A. Krol, K. X. Whipple, K. V. Hodges, K. A. Farley, W. Tang, and Z. Chen (2002). Late Cenozoic evolution of the eastern margin of the Tibetan Plateau: Inferences from $^{40}Ar/^{39}Ar$ and (U-Th)/He thermochronology, *Tectonics* **21,** doi 10.1029/2000TC001246.

Kirby, E., K. X. Whipple, W. Tang, and Z. Chen (2003). Distribution of active rock uplift along the eastern margin of the Tibetan Plateau: Inferences from bedrock channel longitudinal profiles, *J. Geophys. Res.* **108,** doi 10.1029/2001JB000861.

Klinger, Y. (2010). Relation between continental strike-slip earthquake segmentation and thickness of the crust, *J. Geophys. Res.* **115,** 10.1029/2009JB006550.

Klinger, Y., R. Michel, and G. C. P. King (2006). Evidence for an earthquake barrier model from $M_w \sim 7.8$ Kokoxili (Tibet) earthquake slip-distribution, *Earth Planet. Sci. Lett.* **242,** 354–364.

Li, C., R. D. van der Hilst, and A. N. Toksoz (2006). Constraining *P*-wave velocity variations in the upper mantle beneath Southeast Asia, *Phys. Earth Planet. Int.* **154,** 180–195.

Li, H., J. van der Woerd, Z. Wang, X. Fu, L. Hou, J. Si, Z. Qiu, F. Wu, and P. Tapponnier (2008). The M_w 7.9 Wenchuan earthquake of 12 May 2008, Sichuan, China: Surface rupture and oblique right-lateral co-seismic thrusting, *Eos Trans. AGU* **89,** Fall Meet. Suppl., Abstract T33A-2033.

Li, Y., D. Jia, J. H. Shaw, J. Hubbard, A. Lin, M. Wang, L. Luo, H. Li, and L. Wu (2010). Structural interpretation of the co-seismic faults of the Wenchuan earthquake: Three-dimensional modeling of the Longmen Shan fold-and-thrust belt, *J. Geophys. Res.* **115,** doi 10.1029/2009JB006824.

Lin, A., Z. K. Ren, D. Jia, and X. J. Wu (2009). Co-seismic thrusting rupture and slip distribution produced by the 2008 M_w 7.9 Wenchuan earthquake, China, *Tectonophysics* **417,** 203–215.

Liu-Zeng, J., Z. Zhang, L. Wen, P. Tapponnier, J. Sun, X. Xing, G. Hu, Q. Xu, L. Zeng, L. Ding, C. Ji, K. W. Hudnut, and J. van der Woerd (2009). Co-seismic ruptures of the 12 May 2008, M_s 8.0 Wenchuan earthquake, Sichuan: East–west crustal shortening on oblique, parallel thrusts along the eastern edge of Tibet, *Earth Planet. Sci. Lett.* **286,** 355–370.

Mallet, J. L. (1992). Discrete smooth interpolation in geometric modeling, *Comput. Aided Des.* **24,** 178–191.

Matte, P. (1986). Tectonics and plate tectonics model for the Variscan belt of Europe, *Tectonophysics* **126,** 329–374.

Meade, B. J. (2007). Present-day kinematics at the India-Asia collision zone, *Geology* **35,** 81–84.

Meyer, B., P. Tapponnier, L. Bourjot, F. Métivier, Y. Gaudemer, G. Peltzer, G. Shunmin, and C. Zhitai (1998). Crustal thickening in Gansu-Ginghai, lithospheric mantle subduction, and oblique, strike-slip controlled growth of the Tibet plateau, *Geophys. J. Int.* **135,** 1–47.

Parsons, T., C. Ji, and E. Kirby (2008). Stress changes from the 2008 Wenchuan earthquake and increased hazard in the Sichuan basin, *Nature* **454,** 509–510.

Pei, S., J. Su, H. Zhang, Y. Sun, N. Toksoz, J. Zhau, and H. Liu (2008). Three-dimensional imaging of Longmenshan fault using aftershocks of Wenchuan 8.0 earthquake, Sichuan, China, *Eos Trans. AGU* **89,** Fall Meet. Suppl., Abstract U22B-02.

Peltzer, G., P. Tapponnier, Y. Gaudemer, B. Meyer, S. M. Guo, K. L. Yin, Z. T. Chen, and H. G. Dai (1988). Offsets of late Quaternary morphology, rate of slip, and recurrence of large earthquakes on the Chang Ma fault, Gansu, China, *J. Geophys. Res.* **93,** 7793–7812.

Platt, J. P. (1986). Dynamics of orogenic wedges and the uplift of high-pressure metamorphic rocks, *Geol. Soc. Am. Bull.* **97,** 1037–1053.

Plesch, A., J. H. Shaw, C. Benson, W. A. Bryant, S. Carena, M. Cooke, J. Dolan, G. Fuis, E. Gath, L. Grant, E. Hauksson, T. Jordan, M. Kamerling, M. Legg, S. Lindvall, H. Magistrale, C. Nicholson, N. Niemi, M. Oskin, S. Perry, G. Planansky, T. Rockwell, P. Shearer, C. Sorlien, P. Süss, J. Suppe, J. Treiman, and R. Yeats (2007). Community fault model (CFM) for southern California, *Bull. Seismol. Soc. Am.* **97,** 1793–1802.

Richardson, N. J., A. L. Densmore, D. Seward, A. Fowler, M. Wipf, M. A. Ellis, L. Yong, and Y. Zhang (2008). Extraordinary denudation in the Sichuan Basin: Insights from low-temperature thermochronology adjacent to the eastern margin of the Tibetan Plateau, *J. Geophys. Res.* **113,** doi 10.1029/2006JB004739.

Ritz, J.-F., D. Bourles, E. T. Brown, S. Carretier, J. Chery, B. Enhtuvshin, P. Galsan, C. Finkel, T. C. Hanks, K. J. Kendrick, H. Philip, G. Raisbeck, A. Schlupp, D. P. Schwartz, and F. Yiou (2003). Late Pleistocene to Holocene slip rates for the Gurvan Bulag thrust fault (Gobi-Altay, Mongolia) estimated with ^{10}Be dates, *J. Geophys. Res.* **108,** doi 10.1029/2001JB000553.

Royden, L. H., B. C. Burchfiel, R. W. King, E. Wang, Z. Chen, F. Shen, and Y. Liu (1997). Surface deformation and lower crustal flow in eastern Tibet, *Science* **276,** 788–790.

Shaw, J. H., C. Connors, and J. Suppe (2005). *Seismic interpretation of contractional fault-related folds: An AAPG seismic atlas*, Am. Assoc. Pet. Geol., Studies in Geology, #53, 157 pp.

Shen, Z. K., J. N. Lu, M. Wang, and R. Bürgmann (2005). Contemporary crustal deformation around the southeast borderland of the Tibetan Plateau, *J. Geophys Res.* **110,** doi 10.1029/2004JB003421.

Shen, Z. K., J. B. Sun, P. Z. Zhang, Y. G. Wan, M. Wang, R. Bürgmann, Y. H. Zeng, W. J. Gan, H. Liao, and Q. L. Wang (2009). Slip maxima at fault junctions and rupturing of barriers during the 2008 Wenchuan earthquake, *Nature Geoscience* **2,** 718–724.

Sladen, A. (2008). Preliminary Results 05/12/2008 (M_w 7.9), East Sichuan, http://www.tectonics.caltech.edu/slip_history/2008_e_sichuan/e_sichuan.html, last accessed 13 October 2009.

Spotila, J. A., and K. Sieh (1995). Geologic investigations of a slip gap in the surficial ruptures of the 1992 Landers earthquake, Southern California, *J. Geophys. Res.* **100,** 543–559.

Stone, R. (2008). Geophysics: An unpredictably violent fault, *Science* **320,** 1578–1580.

Suppe, J. (1983). Geometry and kinematics of fault-bend folding, *Am. J. Sci.* **283,** 684–721.

Suppe, J. (1984). *Principles of Structural Geology*, Prentice Hall, New York, 155 pp.

Suppe, J. (2007). Absolute fault and crustal strength from wedge tapers, *Geology* **35,** 1127–1130.

Tapponnier, P., and P. Molnar (1977). Active faulting and tectonics in China, *J. Geophys. Res.* **82,** 2905–2930.

Tapponnier, P., Z. Q. Xu, F. Roger, B. Meyer, N. Arnaud, G. Wittlinger, and J. S. Yang (2001). Oblique stepwise rise and growth of the Tibet plateau, *Science* **294,** 1671–1677.

Wesnousky, S. (2006). Predicting the endpoints of earthquake ruptures, *Nature* **444,** 358–360.

Wesnousky, S. (2008). Displacement and geometrical characteristics of earthquake surface ruptures: Issues and implications for seismic-hazard analysis and the process of earthquake rupture, *Bull. Seismol. Soc. Am.* **98,** 1609–1632.

Xu, X., X. Wen, G. Yu, G. Chen, Y. Klinger, J. Hubbard, and J. H. Shaw (2009). Coseismic reverse- and oblique-slip surface faulting generated by the 2008 M_w 7.9 Wenchuan earthquake, China, *Geology* **27,** 515–518.

Zhang, P., F. Mao, and D. B. Slemmons (1999). Rupture terminations and size of segment boundaries from historical earthquake ruptures in the Basin and Range Province, *Tectonophysics* **308,** 37–52.

Department of Earth and Planetary Sciences
Harvard University
20 Oxford St.
Cambridge, Massachusetts 02138
jhubbard@fas.harvard.edu
shaw@eps.harvard.edu
(J.H., J.H.S.)

Institut de Physique du Globe de Paris
75005 Paris, France
klinger@ipgp.jussieu.fr
(Y.K.)

Manuscript received 27 October 2009